Modeling of a Diesel Engine with Intake Throttle, VGT, and EGR

Johan Wahlström and Lars Eriksson

Vehicular systems
Department of Electrical Engineering
Linköpings universitet, SE-581 83 Linköping, Sweden
WWW: www.vehicular.isy.liu.se
E-mail: {johwa, larer}@isy.liu.se
Report: LiTH-ISY-R-2976

November 12, 2010

Abstract

A mean value model of a diesel engine with intake throttle, VGT, and EGR is developed, parameterized, and validated. The intended model applications are system analysis, simulation, and development of model-based control systems. The goal is to construct a model that describes the gas flow dynamics including the dynamics in the intercooler pressure, manifold pressures, turbocharger, EGR, and actuators with few states in order to have short simulation times. An investigation of model complexity and descriptive capabilities is performed, resulting in a model that has only eleven states. To tune and validate the model, stationary and dynamic measurements have been performed in an engine laboratory at Scania CV AB. All the model parameters are estimated automatically using weighted least squares optimization of both the sub-models and the complete model.

Dynamic measurements and simulations show that the proposed model captures the essential system properties, i.e. non-minimum phase behaviors, overshoots, and sign reversals. Validations of the entire model show that the mean value of all absolute relative errors for all measured outputs are equal to 7.4 %.

A system analysis of the proposed model is performed in order to obtain insight into a VGT and EGR control problem where the goal is to control the performance variables oxygen fuel ratio λ_O and EGR-fraction x_{egr}. Step responses over the entire operating region show that the channels VGT to λ_O, EGR to λ_O, and VGT to x_{egr} have sign reversals.

Contents

1 Introduction

Legislated emission limits for heavy duty trucks are constantly reduced. To fulfill the requirements, technologies like Exhaust Gas Recirculation (EGR) systems, Variable Geometry Turbochargers (VGT), and intake throttle have been introduced. The primary emission reduction mechanisms utilized to control the emissions are that NO_x can be reduced by increasing the intake manifold EGR-fraction x_{egr} and smoke can be reduced by increasing the oxygen/fuel ratio λ_O [15]. Therefore, it is natural to choose x_{egr} and λ_O as the main performance variables. However x_{egr} and λ_O depend in complicated ways on the actuation of the EGR, VGT, and intake throttle. It is therefore necessary to have coordinated control of the EGR, VGT, and intake throttle to reach the legislated emission limits in NO_x and smoke. When developing and validating a controller for this system, it is desirable to have a model that describes the system dynamics and the nonlinear effects that are important for gas flow control. For example in [20], [19], and [24] it is shown that this system has non-minimum phase behaviors, overshoots, and sign reversals. Therefore, the objective of this report is to construct a mean value diesel engine model, from actuator input to system output, that captures these properties. The intended usage of the model are system analysis, simulation and development of model-based control systems. The model shall describe the dynamics in the intercooler pressure, the manifold pressures, turbocharger, EGR, and actuators with few states in order to have short simulation times.

Some few models have been published for diesel engines with EGR, VGT, and intake throttle [4, 12, 11]. However, they do not investigate how steps in the intake throttle affect the system. Further, there are several models with different selections of states and complexity that been published for diesel engines with only EGR and VGT, and they are summarized in the following way. A third order model that describes the intake and exhaust manifold pressure and turbocharger dynamics is developed in [16]. The model in [19] has 6 states describing intake and exhaust manifold pressure and temperature dynamics, and turbocharger and compressor mass flow dynamics. A 7:th order model that describes intake and exhaust manifold pressure, temperature, and air-mass fraction dynamics, and turbocharger dynamics is proposed in [1]. These dynamics are also described by the 7:th order models in [16, 20, 24] where burned gas fraction is used instead of air-mass fraction in the manifolds. Another model that describes these dynamics is the 9:th order model in [23] that also has two states for the actuator dynamics. Finally, the eight order model in [25] has five states for the intake and exhaust manifold pressure and air-mass fraction, and turbocharger speed, one state for the VGT-actuator, and two states for the EGR-actuator to describe an overshoot. The models described above are lumped parameter models. Other model families, that have considerably more states are those based on one-dimensional gas dynamics, for example GT-POWER and Ricardo WAVE models.

The model proposed here has eleven states: intercooler, intake manifold, and exhaust manifold pressures, oxygen mass fraction in the intake and exhaust manifold, exhaust manifold temperature, turbocharger speed, and four states describing the actuator dynamics. In order to have a low number of tuning parameters, flows and efficiencies are modeled based upon physical relationships and parametric models instead of look-up tables. The model is implemented in

MATLAB/SIMULINK using a component library, see Appendix B.

1.1 Outline

The structure of the model as well as the tuning and the validation data are described in Sec. 1.2 to 1.6. Model equations and model tuning are described for each sub-model in Sec. 2 to 6. Sec. 7 describes the optimization of the model parameters and the model validation. A system analysis of the proposed model is performed in Sec. 8.

1.2 Selection of number of states

The model has eleven states: intercooler, intake manifold, and exhaust manifold pressures (p_{ic}, p_{im}, and p_{em}), oxygen mass fraction in the intake and exhaust manifold (X_{Oim} and X_{Oem}), exhaust manifold temperature (T_{em}), turbocharger speed (ω_t), and four states describing the actuator dynamics for the three control signals (u_{egr}, u_{vgt}, and u_{th}) where there are two states for the EGR-actuator to describe an overshoot. These states are collected in a state vector x

$$x = (p_{ic} \quad p_{im} \quad p_{em} \quad T_{em} \quad X_{Oim} \quad X_{Oem} \quad \omega_t \quad \tilde{u}_{egr1} \quad \tilde{u}_{egr2} \quad \tilde{u}_{vgt} \quad \tilde{u}_{th})^T \tag{1}$$

Descriptions of the nomenclature, the variables and the indices can be found in Appendix A and the structure of the model can be seen in Fig. 1.

The states p_{ic}, p_{im}, p_{em}, T_{em}, and ω_t describe the main dynamics and the most important system properties, such as non-minimum phase behaviors, overshoots, and sign reversals. In order to model the dynamics in the oxygen/fuel ratio λ_O, the states X_{Oim} and X_{Oem} are used. Finally, the states $\tilde{u}_{egr1}$, $\tilde{u}_{egr2}$, $\tilde{u}_{vgt}$, and $\tilde{u}_{th}$ describe the actuator dynamics where the EGR-valve actuator model has two states ($\tilde{u}_{egr1}$ and $\tilde{u}_{egr2}$) in order to describe an overshoot in the actuator.

Many models in the literature, that approximately have the same complexity as the model proposed here, use three states for the intake manifold and two states for the intercooler in order to describe the temperature dynamics [16, 20, 23, 4]. However, the model proposed here uses only two states for the intake manifold and one state for the intercooler.

Model extensions are investigated in [25] showing that inclusion of temperature states in the intake manifold and intercooler has only minor effects on the dynamics in flows and pressures. However, the temperature dynamics in the exhaust manifold is important to model since this dynamics has effects on the dynamics in EGR and turbine flow during steps in fuel injection.

1.3 Model structure

It is important that the model can be utilized both for different vehicles and for engine testing and calibration. In these situations the engine operation is defined by the rotational speed n_e, for example given as an input from a drivecycle, and therefore it is natural to parameterize the model using engine speed. The resulting model is thus expressed in state space form as

$$\dot{x} = f(x, u, n_e) \tag{2}$$

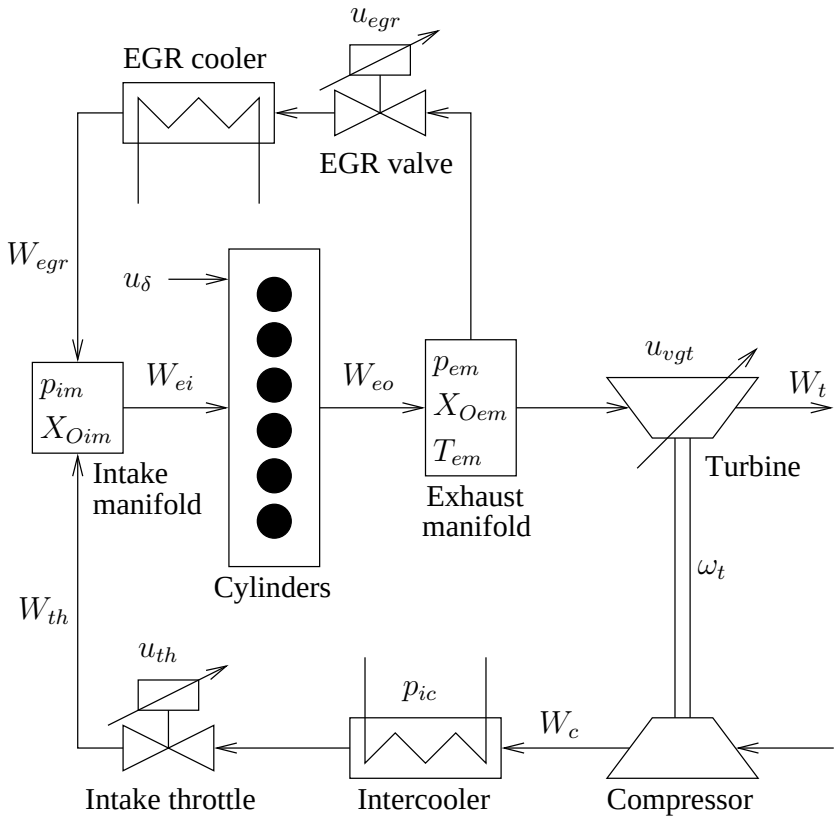

Figure 1: A model structure of the diesel engine. It has seven main states related to the engine (p_{ic}, p_{im}, p_{em}, T_{em}, X_{Oim}, X_{Oem}, and ω_t). In addition, there are four states for actuator dynamics ($\tilde{u}_{egr1}$, $\tilde{u}_{egr2}$, $\tilde{u}_{vgt}$, and $\tilde{u}_{th}$).

where the engine speed n_e is considered as a measured disturbance, and u is the control input vector

$$u = (u_\delta \quad u_{egr} \quad u_{vgt} \quad u_{th})^T \tag{3}$$

which contains mass of injected fuel u_δ, EGR-valve position u_{egr}, VGT actuator position u_{vgt}, and intake throttle position u_{th}. The EGR-valve, VGT, and intake throttle are closed when $u_{egr} = 0\,\%$, $u_{vgt} = 0\,\%$, and $u_{th} = 0\,\%$, and they are open when $u_{egr} = 100\,\%$, $u_{vgt} = 100\,\%$, and $u_{th} = 100\,\%$.

1.4 Measurements

To tune and validate the model, stationary and dynamic measurements have been performed in an engine laboratory at Scania CV AB, and these are described below.

1.4.1 Stationary measurements

The stationary data consists of measurements at stationary conditions in 3769 operating points, that are scattered over a large operating region covering dif-

Table 1: Measured variables during stationary measurements.

Variable	Description	Unit
n_e	Rotational engine speed	rpm
n_t	Rotational turbine speed	rpm
p_{amb}	Ambient pressure	Pa
p_{em}	Exhaust manifold pressure	Pa
p_{ic}	Intercooler pressure	Pa
p_{im}	Intake manifold pressure	Pa
T_{amb}	Ambient temperature	K
T_c	Temperature after compressor	K
T_{em}	Exhaust manifold temperature	K
T_{im}	Intake manifold temperature	K
T_t	Temperature after turbine	K
u_{egr}	EGR control signal. 0 - closed, 100 - open	%
u_{vgt}	VGT control signal. 0 - closed, 100 - open	%
u_{th}	Intake throttle control signal. 0 - closed, 100 - open	%
u_δ	Injected amount of fuel	$mg/cycle$
W_c	Compressor mass flow	kg/s

ferent loads, speeds, EGR, VGT, and throttle positions. The fuel injection u_δ has 5 different values between 0-230 mg/cycle, n_e has 5 different values between 500-2000 rpm, u_{egr} has 50 different values between 0-100 %, u_{vgt} has 34 different values between 7-100 %, and u_{th} has 84 different values between 5-100 %. The variables that were measured during stationary measurements can be seen in Tab. 1.

75 % of the stationary measurements are used for tuning of parameters in static models. The rest of the stationary measurements (25 %) are used for validation of the static models. The tuning and the validation data are selected so that both these data sets cover a large operating region.

1.4.2 Dynamic measurements

The dynamic measurements consist of two different data sets. The first data set consists of measurements with steps in EGR control signal, VGT control signal, intake throttle control signal, fuel injection, and engine speed in 139 different operating points that are scattered over a large operating region. The steps in EGR position are performed between 3 different values between 0-100 %, the steps in VGT position are performed between 4 different values between 7-100 %, the steps in intake throttle position are performed between 4 different values between 0-100 %, the steps in fuel injection are performed between 3 different values between 20-200 mg/cycle, and the steps in engine speed are performed between 3 different values between 500-2000 rpm. This data set is used for tuning of parameters in dynamic models.

The second data set consists of measurements from the World Harmonized Transient Cycle (WHTC) [7] where a complete controller is used that have been provided by industry. This data set is used for validation of the complete model.

The variables that were measured during dynamic measurements can be seen in Tab. 2. Further, in [25] the sensor dynamics are investigated showing that

Table 2: Measured variables during dynamic measurements.

Variable	Description	Unit
n_e	Rotational engine speed	rpm
n_t	Rotational turbine speed	rpm
p_{amb}	Ambient pressure	Pa
p_{em}	Exhaust manifold pressure	Pa
p_{ic}	Intercooler pressure	Pa
p_{im}	Intake manifold pressure	Pa
T_{amb}	Ambient temperature	K
$\tilde{u}_{th}$	Intake throttle position 0 - closed, 100 - open	%
u_{th}	Intake throttle control signal 0 - closed, 100 - open	%
u_{egr}	EGR control signal 0 - closed, 100 - open	%
u_{vgt}	VGT control signal 0 - closed, 100 - open	%
u_δ	Injected amount of fuel	$mg/cycle$
W_c	Compressor mass flow	kg/s

the dynamics visible in the experimental data is due to the system dynamics, this is due to that the sensors are much faster than the system dynamics.

1.5 Parameter estimation and validation

Model parameters are estimated in four steps. Firstly, the static parameters are initialized using least squares optimization for each sub-model in Sec. 2 to 6 and using 75% of the data from stationary measurements. Secondly, the static parameters are finally estimated using least squares optimization for each sub-model and for the complete model and using 75% of the data from stationary measurements. In the second step the static parameters are initialized using the method in the first step.

Thirdly, the actuator parameters for the intake throttle are estimated using least squares optimization for the actuator model and using the measurements from the first dynamic data set in Sec. 1.4.2 that only consist of steps in throttle position. The parameters values for the EGR and VGT actuator models are set to be the same as the model in [25]. Fourthly, the intercooler volume, the manifold volumes, and the turbocharger inertia are estimated using least squares optimization for the complete model and using all the measurements from the first dynamic data set in Sec. 1.4.2.

Static sub-models are validated using 25 % of the stationary measurements. The complete model is validated both in stationary and dynamic conditions using the second data set in Sec. 1.4.2.

1.6 Error

Errors are calculated and used to evaluate the tuning and the validation of the model. Two different errors are used: relative errors and errors. Relative errors

between a measured variable y_{meas} and a modeled variable y_{mod} are calculated as

$$\text{relative error}(i) = \frac{y_{meas}(i) - y_{mod}(i)}{y_{meas}(i)} \tag{4}$$

and errors between a measured variable y_{meas} and a modeled variable y_{mod} are calculated as

$$\text{error}(i) = y_{meas}(i) - y_{mod}(i) \tag{5}$$

where i is an operating point for a stationary measurement or a time sample for a dynamic measurement. Relative errors are used for all signals except for the EGR-fraction x_{egr} and the exhaust manifold temperature T_{em} where errors are used.

2 Control volumes

The diesel engine model consist of three control volumes: intercooler volume, intake manifold, and exhaust manifold.

2.1 Intercooler volume

The intercooler volume is modeled as a dynamic system with one state, the intercooler pressure. The standard isothermal model [15], that is based upon mass conservation, the ideal gas law, and that the intercooler temperature is constant, gives the differential equation for the intercooler pressure

$$\frac{d}{dt}p_{ic} = \frac{R_a\, T_{im}}{V_{ic}} \sum_i W_i \tag{6}$$

$$W_1 = W_c \tag{7}$$

$$W_2 = -W_{th} \tag{8}$$

where R_a is the ideal gas constant in air and V_{ic} is the intercooler volume. The temperature out from the intercooler is assumed to be constant and equal to the intake manifold temperature T_{im}. The mass flows W_{th} and W_c will be described in Sec. 3 and 6.3.

2.2 Intake manifold

The intake manifold pressure is modeled in the same way as the intercooler pressure

$$\frac{d}{dt}p_{im} = \frac{R_a\, T_{im}}{V_{im}} \sum_i W_i \tag{9}$$

$$W_1 = W_{th} \tag{10}$$

$$W_2 = W_{egr} \tag{11}$$

$$W_3 = -W_{ei} \tag{12}$$

$$\tag{13}$$

where V_{im} is the intake manifold volume and the mass flows W_{ei} and W_{egr} will be described in Sec. 4.1 and 5. In (9) it is assumed that the intake manifold

temperature T_{im} is constant, i.e. the EGR-mass flow does not affect T_{im} which is reasonable since there is an EGR-cooler that cools the EGR gases and this EGR-cooler has the same cooling temperature as the intercooler. An alternative model has been investigated where the EGR-cooler is not ideal, i.e. the EGR gases into the intake manifold has a temperature that is higher than the cooling temperature, and where a dynamic adiabatic model for mixing of temperatures in the intake manifold is used. However, this alternative model does not improve the model quality on the tuning data. Therefore, the isothermal model (9) with constant temperature is proposed.

The EGR fraction in the intake manifold is calculated as

$$x_{egr} = \frac{W_{egr}}{W_{th} + W_{egr}} \tag{14}$$

Note that the EGR gas also contains oxygen that affects the oxygen fuel ratio in the cylinder. This effect is considered by modeling the oxygen concentration X_{Oim} in the intake manifold. This concentration is defined in the same way as in [24]

$$X_{Oim} = \frac{m_{Oim}}{m_{totim}} \tag{15}$$

where m_{Oim} is the oxygen mass, and m_{totim} is the total mass in the intake manifold. Differentiating X_{Oim} and using mass conservation [24] give the following differential equation

$$\frac{d}{dt}X_{Oim} = \frac{R_a\, T_{im}}{p_{im}\, V_{im}} \sum_i (X_{O,i} - X_{Oim}) \max(W_i, 0) \tag{16}$$

$$X_{O,1} = X_{Oc} \tag{17}$$

$$X_{O,2} = X_{Oem} \tag{18}$$

$$X_{O,3} = 0 \tag{19}$$

where X_{Oc} is the constant oxygen concentration passing the compressor, intercooler, and the intake throttle i.e. air with $X_{Oc} = 23.14\%$, and X_{Oem} is the oxygen concentration in the exhaust manifold.

Another way to consider the oxygen in the EGR gas, is to model the burned gas ratio in the intake manifold which is a frequent choice for state in many papers [16, 20, 23]. The oxygen concentration and the burned gas ratio have exactly the same effect on the oxygen fuel ratio and therefore these states are equivalent.

2.3 Exhaust manifold

In the exhaust manifold it is important to model the temperature dynamics since this dynamics has effects on the dynamics in EGR and turbine flow during steps in fuel injection. Therefore, the following adiabatic model [5, 14] is used that is

based upon mass conversation and the ideal gas law

$$\frac{d}{dt}p_{em} = \frac{R_e\, T_{em}}{V_{em}} \sum_i W_i + \frac{p_{em}}{T_{em}} \frac{d}{dt} T_{em} \tag{20}$$

$$\frac{d}{dt}T_{em} = \frac{R_e\, T_{em}}{p_{em}\, V_{em}\, c_{ve}} (W_{in}\, c_{ve}(T_{em,in} - T_{em}) + R_e(T_{em,in}\, W_{in} - T_{em}\, W_{out})) \tag{21}$$

$$W_{in} = \sum_i \max(W_i, 0) \tag{22}$$

$$W_{out} = \sum_i \max(-W_i, 0) \tag{23}$$

$$W_1 = W_{eo} \tag{24}$$

$$W_2 = -W_{egr} \tag{25}$$

$$W_3 = -W_t \tag{26}$$

where p_{em} is the exhaust manifold pressure, T_{em} is the exhaust manifold temperature, R_e is the ideal gas constant in exhaust gas, V_{em} is the exhaust manifold volume, and c_{ve} is the specific heat capacity at constant volume in exhaust gas. The temperature $T_{em,in}$ into the exhaust manifold will be described in Sec. 4.2 and the mass flows W_{eo} and W_t will be described in Sec. 4.1 and 6.2. In (21) it is assumed that all flows into the exhaust manifold have the temperature $T_{em,in}$, i.e. when there is a back-flow through the EGR-valve ($W_{egr} < 0$) it is assumed that the EGR-flow W_{egr} has the temperature $T_{em,in}$ which is reasonable since $|W_{egr}|$ is small when $W_{egr} < 0$ and consequently this mass flow is heated up very fast by the warm exhaust pipes. An alternative model has been investigated where (21) is extended so that the inlet flows can have different temperatures and that the EGR-mass flow has a temperature that is equal to the cooling temperature of the EGR-cooler. However, this alternative model does not improve the model quality on the tuning data. Therefore, the dynamic exhaust manifold temperature model (21) is proposed.

The oxygen concentration in the exhaust manifold is modeled in the same way as in the intake manifold

$$\frac{d}{dt}X_{Oem} = \frac{R_e\, T_{em}}{p_{em}\, V_{em}} \sum_i (X_{O,i} - X_{Oem}) \max(W_i, 0) \tag{27}$$

$$X_{O,1} = X_{Oe} \tag{28}$$

$$X_{O,2} = X_{Oim} \tag{29}$$

$$X_{O,3} = 0 \tag{30}$$

where X_{Oe} is the oxygen concentration in the exhaust gases coming from the engine cylinders, X_{Oe} will be described in Sec. 4.1.

2.4 Tuning

Tuning parameters

- V_{ic}: Intercooler volume
- V_{im} and V_{em}: manifold volumes

Tuning method

The tuning parameters above are determined using least squares optimization for the complete model and using the first data set in Sec. 1.4.2, see Sec. 7.1 for more details.

3 Intake throttle

The mass flow through the intake throttle is modeled as a compressible flow restriction with variable area [15]

$$W_{th} = \frac{p_{ic}\,\Psi_{th}(\Pi_{th})\,A_{th,max}\,f_{th}(\tilde{u}_{th})}{\sqrt{T_{im}\,R_a}} \tag{31}$$

where

$$\Psi_{th}(\Pi_{th}) = \begin{cases} \Psi^*_{th}(\Pi_{th}) & \text{if } \Pi_{th} \leq \Pi_{th,lin} \\ \Psi^*_{th}(\Pi_{th,lin})\frac{1-\Pi_{th}}{1-\Pi_{th,lin}} & \text{if } \Pi_{th,lin} < \Pi_{th} \end{cases} \tag{32}$$

$$\Psi^*_{th}(\Pi_{th}) = \sqrt{\frac{2\,\gamma_{th}}{\gamma_{th}-1}\left(\Pi_{th}^{2/\gamma_{th}} - \Pi_{th}^{1+1/\gamma_{th}}\right)} \tag{33}$$

To prevent $dW_{th}/d\Pi_{th}$ from reaching $-\infty$ for pressure ratios close to 1, (32) is linearized for pressure ratios above $\Pi_{th,lin}$.

The pressure quotient Π_{th} over the throttle is limited when the flow is choked, i.e. when sonic conditions are reached in the throat, and when $1 < p_{im}/p_{ic}$, i.e. no backflow can occur.

$$\Pi_{th} = \begin{cases} \left(\frac{2}{\gamma_{th}+1}\right)^{\frac{\gamma_{th}}{\gamma_{th}-1}} & \text{if } \frac{p_{im}}{p_{ic}} < \left(\frac{2}{\gamma_{th}+1}\right)^{\frac{\gamma_{th}}{\gamma_{th}-1}} \\ \frac{p_{im}}{p_{ic}} & \text{if } \left(\frac{2}{\gamma_{th}+1}\right)^{\frac{\gamma_{th}}{\gamma_{th}-1}} \leq \frac{p_{im}}{p_{ic}} \leq 1 \\ 1 & \text{if } 1 < \frac{p_{im}}{p_{ic}} \end{cases} \tag{34}$$

The area ratio $f_{th}(u_{th})$ is modeled as [2]

$$f_{th}(\tilde{u}_{th}) = b_{th1}(1 - \cos(\min(a_{th1}\,\tilde{u}_{th} + a_{th2}, \pi))) + b_{th2} \tag{35}$$

Tuning parameters

If γ_{th} in (33) and (34) is chosen to be a physical value $\gamma_{th} = \gamma_a$ and b_{th1}, b_{th2}, a_{th1}, and a_{th2} are chosen to be tuning parameters, the mean absolute relative error between W_{th} and $W_{c,meas}$ will be equal to 2.8 %. One explanation to these model errors is that the maximum effective area $A_{th,max}$ depends on the pressure ratio Π_{th} and this dependency is non-negligible [2]. To consider this dependency, the product $\Psi_{th}(\Pi_{th})\,A_{th,max}(\Pi_{th})$ in (31) is modeled as $\Psi^{\gamma_{th}}_{th}(\Pi_{th})\,A_{th,max}$ where $\Psi^{\gamma_{th}}_{th}(\Pi_{th})$ is the function in (32) where γ_{th} is considered as a tuning parameter and $A_{th,max}$ is a constant [2]. Using this model, the mean absolute relative error between W_{th} and $W_{c,meas}$ is reduced to 2.0 %. Consequently, the throttle mass flow model has the following tuning parameters

- γ_{th}: Specific heat capacity ratio for the gas in the throttle
- b_{th1}, b_{th2}, a_{th1}, and a_{th2}: coefficients in the function for the effective area

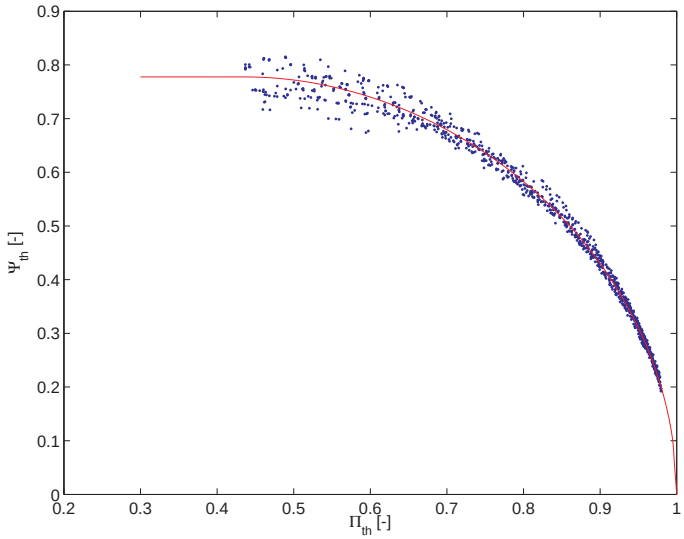

Figure 2: Comparison of calculated points from measurements and a sub-model for the throttle flow W_{th} at steady state showing how different variables in the sub-model depend on each other. Note that this is not a validation of the sub-model since the calculated points for the sub-model depend on the model tuning. The line shows Ψ_{th} (32) as function of pressure quotient Π_{th}. The data points are calculated by solving (31) for Ψ_{th}.

Initialization method

The tuning parameters above are initialized by solving a separable non-linear least-squares problem, see [3] for details about the solution method. The non-linear part of this problem minimizes $(W_{th} - W_{c,meas})^2$ with γ_{th}, a_{th1}, and a_{th2} as the optimization variables. In each iteration in the non-linear least-squares solver, the values for b_{th1} and b_{th2} are set to be the solution of a linear least-squares problem that minimizes $(W_{th} - W_{c,meas})^2$ for the current value of γ_{th}, a_{th1}, and a_{th2}. Points with pressure ratios larger than 0.98 have been omitted in the initialization as the $\Psi_{th}(\Pi_{th})$ function is very sensitive to small changes in Π_{th} in these points, caused by for example pressure sensor errors. The variable W_{th} is described by the model (31). Stationary measurements are used as inputs to the model. The result of the initialization is shown in Fig. 2, 3, and 4 showing that the model describes different variables in the throttle well. Fig. 4 also shows a validation of the throttle mass flow model. The tuning and the validation data give a mean absolute relative error of 2.0 % respectively 2.1 %. The parameters are then tuned according to the method in Sec. 7.1.

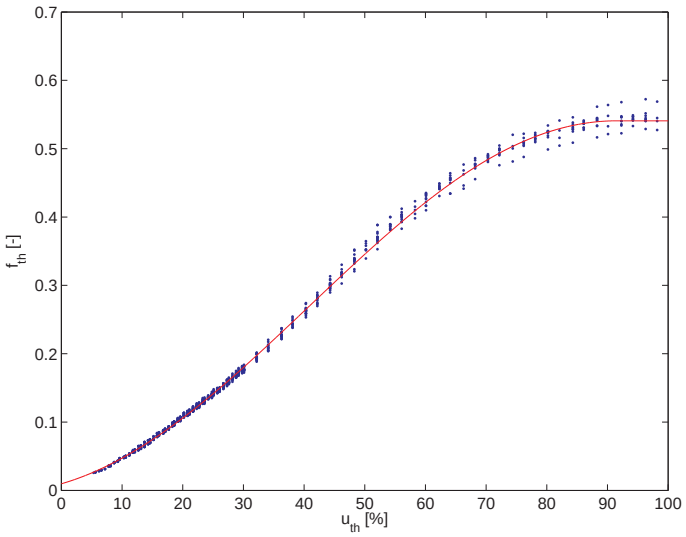

Figure 3: Comparison of calculated points from measurements and a sub-model for the throttle flow W_{th} at steady state showing how different variables in the sub-model depend on each other. Note that this is not a validation of the sub-model since the calculated points for the sub-model depend on the model tuning. The line shows the effective area ratio f_{th} (35) as function of control signal u_{th}. The data points are calculated by solving (31) for f_{th}.

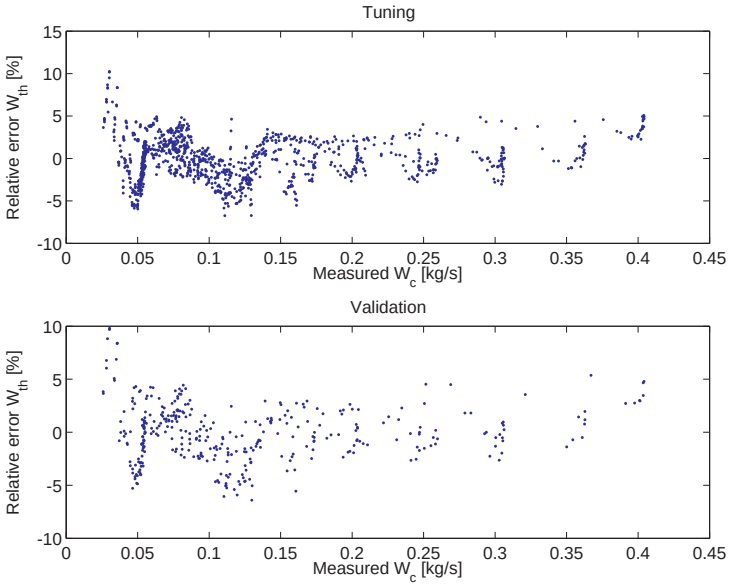

Figure 4: Relative error between modeled throttle flow W_{th} and measured compressor mass flow W_c for the tuning and validation data. The tuning and the validation data give a mean absolute relative error of 2.0 % respectively 2.1 %.

3.1 Throttle actuator

The throttle actuator dynamics is modeled as a first order system with a time delay and a rate limit according to

$$
\begin{aligned}
w_{th} &= \frac{1}{\tau_{th}}(u_{th}(t-\tau_{dth}) - \tilde{u}_{th}) \\
\frac{d}{dt}\tilde{u}_{th} &= \begin{cases} RL_{th} & \text{if } w_{th} > RL_{th} \\ w_{th} & \text{if } -RL_{th} \leq w_{th} \leq RL_{th} \\ -RL_{th} & \text{if } w_{th} < -RL_{th} \end{cases}
\end{aligned}
\tag{36}
$$

Tuning parameters

- τ_{th}: time constant
- τ_{dth}: time delay
- RL_{th}: rate limit

Tuning method

The tuning parameters above are determined by solving a nonlinear least-squares problem that minimizes $(\tilde{u}_{th} - \tilde{u}_{th,meas})^2$ with τ_{th}, τ_{dth}, and RL_{th} as the optimization variables. The variable $\tilde{u}_{th}$ is the model in (36) and $\tilde{u}_{th,meas}$ are the measurements from the first dynamic data set in Sec. 1.4.2 that only consist of steps in throttle position. This data consist of 168 steps in throttle

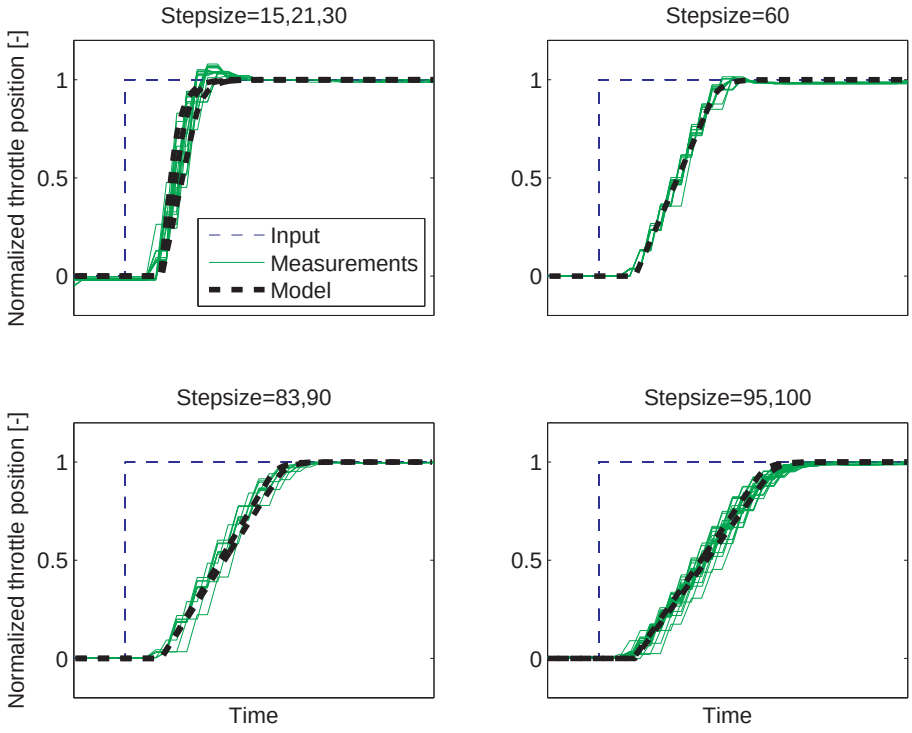

Figure 5: Comparison between throttle actuator dynamic simulation and dynamic tuning data during steps in throttle position.

position with the step sizes 15, 21, 30, 60, 83, 90, 95, and 100 %. These measurements are compared with the step responses of the model (36) in Fig. 5 where all step responses are normalized and shifted in time in order to achieve the same starting point of the input step. Fig. 5 shows that the model describes the actuator well.

4 Cylinder

Three sub-models describe the behavior of the cylinder, these are:

- A mass flow model that describes the gas and fuel flows that enter and leave the cylinder, the oxygen to fuel ratio, and the oxygen concentration out from the cylinder.
- A model of the temperature for the flow into the exhaust manifold
- An engine torque model.

4.1 Cylinder flow

The total mass flow W_{ei} from the intake manifold into the cylinders is modeled using the volumetric efficiency η_{vol} [15]

$$W_{ei} = \frac{\eta_{vol}\, p_{im}\, n_e\, V_d}{120\, R_a\, T_{im}} \tag{37}$$

where p_{im} and T_{im} are the pressure and temperature in the intake manifold, n_e is the engine speed and V_d is the displaced volume. The volumetric efficiency is in its turn modeled as

$$\eta_{vol} = c_{vol1} \frac{r_c - \left(\frac{p_{em}}{p_{im}}\right)^{1/\gamma_e}}{r_c - 1} + c_{vol2}\, W_f^2 + c_{vol3}\, W_f + c_{vol4} \tag{38}$$

where the fuel mass flow W_f into the cylinders is controlled by u_δ, which gives the injected mass of fuel in mg per cycle and cylinder

$$W_f = \frac{10^{-6}}{120}\, u_\delta\, n_e\, n_{cyl} \tag{39}$$

where n_{cyl} is the number of cylinders. The mass flow W_{eo} out from the cylinder is given by the mass balance as

$$W_{eo} = W_f + W_{ei} \tag{40}$$

The oxygen to fuel ratio λ_O in the cylinder is defined as

$$\lambda_O = \frac{W_{ei}\, X_{Oim}}{W_f\, (O/F)_s} \tag{41}$$

where $(O/F)_s$ is the stoichiometric relation between the oxygen and fuel masses. The oxygen to fuel ratio is equivalent to the air fuel ratio which is a common choice of performance variable in the literature [16, 21, 22, 23].

During the combustion, the oxygen is burned in the presence of fuel. In diesel engines $\lambda_O > 1$ to avoid smoke. Therefore, it is assumed that $\lambda_O > 1$ and the oxygen concentration out from the cylinder can then be calculated as the unburned oxygen fraction

$$X_{Oe} = \frac{W_{ei}\, X_{Oim} - W_f\, (O/F)_s}{W_{eo}} \tag{42}$$

Tuning parameters

- c_{vol1}, c_{vol2}, c_{vol3}, and c_{vol4}: volumetric efficiency constants

Initialization method

The tuning parameters c_{vol1}, c_{vol2}, c_{vol3} and c_{vol4} are initialized by solving a linear least-squares problem that minimizes $(W_{ei} - W_{c,meas})^2$ with c_{vol1}, c_{vol2}, c_{vol3} and c_{vol4} as the optimization variables. The variable W_{ei} is the model in (37) to (39). Stationary measurements are used as inputs to the model during the initialization. Measurements with $u_{egr} > 0$ have been omitted in

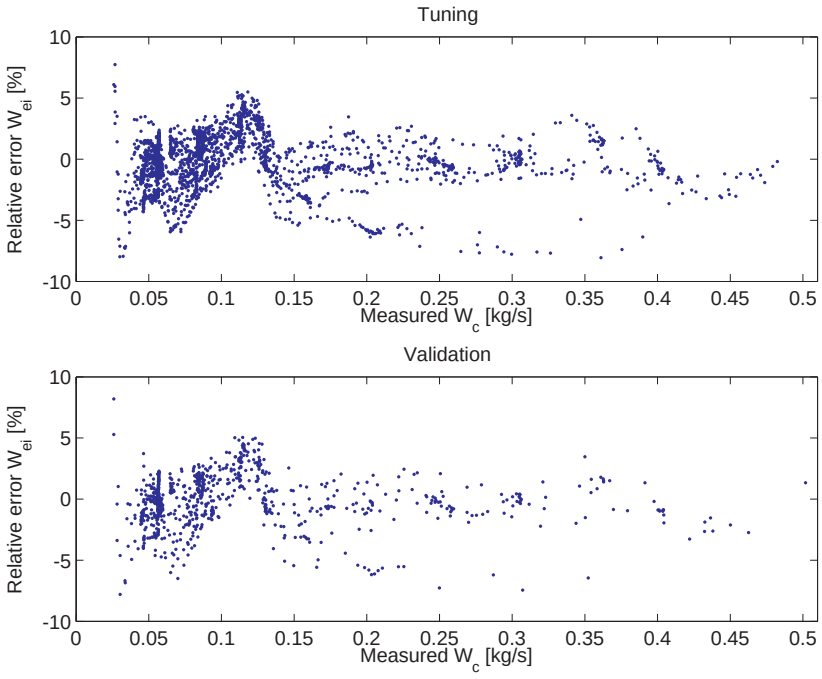

Figure 6: Relative error between modeled mass flow W_{ei} into the cylinders and measured compressor mass flow W_c for the tuning and validation data. The tuning and the validation data give a mean absolute relative error of 1.6 % respectively 1.7 %.

the initialization as the EGR-mass flow is not measured. The result of the initialization and the validation are shown in Fig. 6 which shows that the model describes the cylinder mass flow well. The tuning and the validation data give a mean absolute relative error of 1.6 % respectively 1.7 %. The parameters are then tuned according to the method in Sec. 7.1.

4.2 Exhaust manifold temperature

The model of the temperature for the flow into the exhaust manifold consists of a model for the cylinder out temperature and a model for the heat losses in the exhaust pipes.

Cylinder out temperature

The cylinder out temperature T_e is modeled in the same way as in [18]. This approach is based upon the first law of thermodynamics and an energy balance of the cylinder that give the cylinder out temperature

$$T_e = T_{im} + \frac{q_{HV}\, f_{Te}(W_f, n_e)}{c_{pe}\, W_{eo}} \tag{43}$$

where $f_{Te}(W_f, n_e)$ is modeled as

$$\begin{aligned} f_{Te}(W_f, n_e) =& f_{TeWf}(W_f) \cdot f_{Tene}(n_e) \cdot \min(\lambda_O, 1) \\ f_{TeWf}(W_f) =& c_{fTeWf1}\, W_{f,norm}^3 + c_{fTeWf2}\, W_{f,norm}^2 + \\ & c_{fTeWf3}\, W_{f,norm} + c_{fTeWf4} \\ f_{Tene}(n_e) =& c_{fTene1}\, n_{e,norm}^2 + c_{fTene2}\, n_{e,norm} + 1 \end{aligned} \tag{44}$$

where

$$W_{f,norm} = W_f \cdot 100, \quad n_{e,norm} = \frac{n_e}{1000} \tag{45}$$

The cylinder out temperature model (43)-(45) is a quite simple model. A more complicated model has been investigated and this model is proposed in [26] and it is based upon ideal gas Seliger cycle. However, this model does not improve the model quality on the tuning data and this model requires also an implementation of a fixed point iteration. Therefore, the cylinder out temperature model (43)-(45) is proposed.

Heat losses in the exhaust pipes

The cylinder out temperature model above does not describe the exhaust manifold temperature completely due to heat losses in the exhaust pipes between the cylinder and the exhaust manifold. Therefore the next step is to include a sub-model for these heat losses.

This temperature drop is modeled in the same way as Model 1, presented in [8], where the temperature drop is described as a function of mass flow out from the cylinder

$$T_{em,in} = T_{amb} + (T_e - T_{amb})\, e^{-\frac{h_{tot}\,\pi\, d_{pipe}\, l_{pipe}\, n_{pipe}}{W_{eo}\, c_{pe}}} \tag{46}$$

where T_{amb} is the ambient temperature, h_{tot} the total heat transfer coefficient, d_{pipe} the pipe diameter, l_{pipe} the pipe length and n_{pipe} the number of pipes.

Tuning parameters

- c_{fTeWf1}, c_{fTeWf2}, c_{fTeWf3}, c_{fTeWf4}, c_{fTene1}, and c_{fTene2} coefficients in the polynomial functions (44)
- h_{tot}: the total heat transfer coefficient

Initialization method

The tuning parameters above are initialized by solving a separable non-linear least-squares problem, see [3] for details about the solution method. The non-linear part of this problem minimizes $(T_{em,in} - T_{em,meas})^2$ with c_{fTene1}, c_{fTene2}, and h_{tot} as the optimization variables. In each iteration in the non-linear least-squares solver, the values for c_{fTeWf1}, c_{fTeWf2}, c_{fTeWf3}, and c_{fTeWf4} are set to be the solution of a linear least-squares problem that minimizes $(T_e - T_{im} - (T_{e,meas} - T_{im,meas}))^2$ for the current values of c_{fTene1}, c_{fTene2}, and h_{tot}. The variable $T_{em,in}$ is the model in (43) and (46) with stationary measurements as inputs to the model, and $T_{em,meas}$ is a stationary measurement. The expression $T_e - T_{im}$ is calculated by solving (43) for $T_e - T_{im}$, $T_{e,meas}$ is calculated from

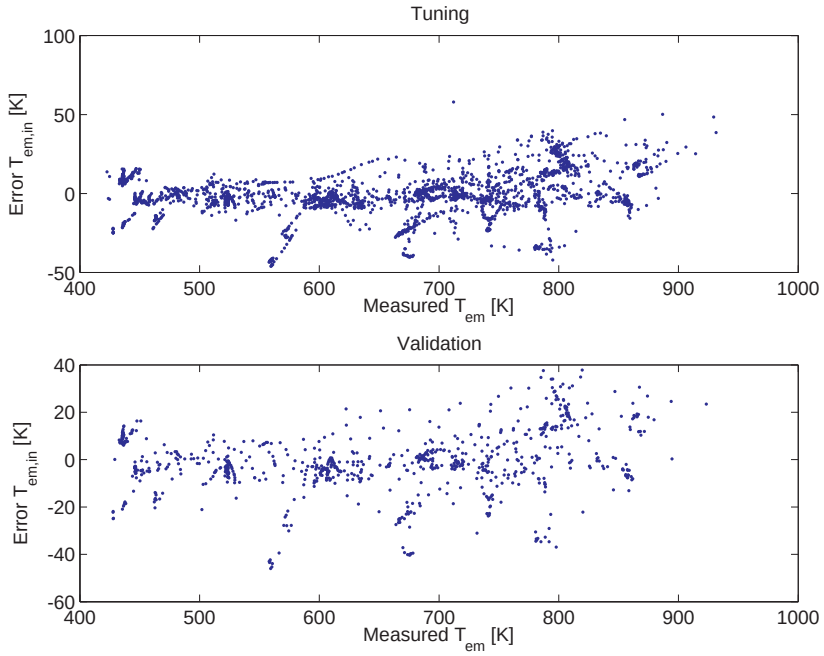

Figure 7: Error between modeled temperature $T_{em,in}$ for the flow into the exhaust manifold and measured exhaust manifold temperature T_{em} for the tuning and validation data. The tuning and the validation data give a mean absolute error of 9.5 K respectively 9.4 K.

measurements by solving (46) for T_e, and $T_{im,meas}$ is a stationary measurement. The result of the initialization and the validation are shown in Fig. 7 which shows that the model describes the temperature for the flow into the exhaust manifold well. The tuning and the validation data give a mean absolute error of 9.5 K respectively 9.4 K. The parameters are then tuned according to the method in Sec. 7.1.

4.3 Engine torque

The torque produced by the engine M_e is modeled using three different engine components; the gross indicated torque M_{ig}, the pumping torque M_p, and the friction torque M_{fric} [15].

$$M_e = M_{ig} - M_p - M_{fric} \tag{47}$$

The pumping torque is modeled using the intake and exhaust manifold pressures.

$$M_p = \frac{V_d}{4\,\pi}\,(p_{em} - p_{im}) \tag{48}$$

The gross indicated torque is coupled to the energy that comes from the fuel

$$M_{ig} = \frac{u_\delta\, 10^{-6}\, n_{cyl}\, q_{HV}\, \eta_{ig}}{4\,\pi} \tag{49}$$

Assuming that the engine is always running at optimal injection timing, the gross indicated efficiency η_{ig} is modeled as

$$\eta_{ig} = \eta_{igch} \left(1 - \frac{1}{r_c^{\gamma_{cyl}-1}} \right) \tag{50}$$

where the parameter η_{igch} is estimated from measurements, r_c is the compression ratio, and γ_{cyl} is the specific heat capacity ratio for the gas in the cylinder. The friction torque is assumed to be a quadratic polynomial in engine speed [15].

$$M_{fric} = \frac{V_d}{4\,\pi} 10^5 \, \left(c_{fric1}\, n_{eratio}^2 + c_{fric2}\, n_{eratio} + c_{fric3} \right) \tag{51}$$

where

$$n_{eratio} = \frac{n_e}{1000} \tag{52}$$

Tuning parameters

- η_{igch}: combustion chamber efficiency
- c_{fric1}, c_{fric2}, c_{fric3}: coefficients in the polynomial function for the friction torque

Tuning method

The values of the tuning parameters above are the same as for the engine torque model in [25].

5 EGR-valve

The EGR-valve model consists of sub-models for the EGR-valve mass flow and the EGR-valve actuator.

5.1 EGR-valve mass flow

The mass flow through the EGR-valve is modeled as a simplification of a compressible flow restriction with variable area [15].

The mass flow through the restriction is

$$W_{egr} = \begin{cases} \frac{A_{egr}\, p_{em}\, \Psi_{egr}\left(\frac{p_{im}}{p_{em}}\right)}{\sqrt{T_{em}\, R_e}} & \text{if } p_{em} \geq p_{im} \\ -\frac{A_{egr}\, p_{im}\, \Psi_{egr}\left(\frac{p_{em}}{p_{im}}\right)}{\sqrt{T_{egr,cool}\, R_a}} & \text{if } p_{em} < p_{im} \end{cases} \tag{53}$$

where

$$\Psi_{egr}(\Pi_{egr}) = \sqrt{\frac{2\,\gamma_e}{\gamma_e - 1} \left(\Pi_{egr}^{2/\gamma_e} - \Pi_{egr}^{1+1/\gamma_e} \right)} \tag{54}$$

Measurement data shows that (54) does not give a sufficiently accurate description of the EGR flow. Pressure pulsations in the exhaust manifold or the influence of the EGR-cooler could be two different explanations for this phenomenon. In order to maintain the density influence $(p/(\sqrt{T\,R}))$ in (53) and

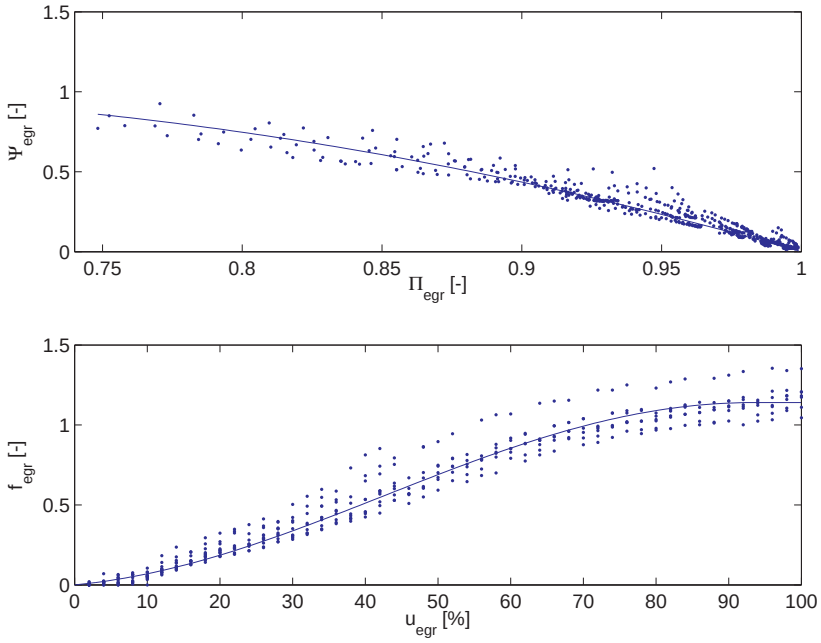

Figure 8: Comparison of calculated points from measurements and two sub-models for the EGR flow W_{egr} at steady state showing how different variables in the sub-models depend on each other. Note that this is not a validation of the sub-models since the calculated points for the sub-models depend on the model tuning. **Top:** The line shows Ψ_{egr} (55) as function of pressure quotient Π_{egr}. The data points are calculated by solving (53) for Ψ_{egr}. **Bottom:** The line shows the effective area ratio f_{egr} (59) as function of control signal u_{egr}. The data points are calculated by solving (53) for f_{egr}.

the simplicity in the model, the function Ψ_{egr} is instead modeled as a parabolic function (see Fig. 8 where Ψ_{egr} is plotted as function of Π_{egr}).

$$\Psi_{egr}(\Pi_{egr}) = 1 - \left(\frac{1 - \Pi_{egrlim}(\Pi_{egr})}{1 - \Pi_{egropt}} - 1 \right)^2 \tag{55}$$

The pressure quotient Π_{egr} over the valve is limited when the flow is choked, i.e. when sonic conditions are reached in the throat.

$$\Pi_{egrlim}(\Pi_{egr}) = \begin{cases} \Pi_{egropt} & \text{if } \Pi_{egr} < \Pi_{egropt} \\ \Pi_{egr} & \text{if } \Pi_{egr} \geq \Pi_{egropt} \end{cases} \tag{56}$$

For a compressible flow restriction, the standard model for Π_{egropt} is

$$\Pi_{egropt} = \left(\frac{2}{\gamma_e + 1} \right)^{\frac{\gamma_e}{\gamma_e - 1}} \tag{57}$$

but the accuracy of the EGR flow model is improved by replacing the physical value of Π_{egropt} in (57) with a tuning parameter [2].

The effective area

$$A_{egr} = A_{egrmax}\, f_{egr}(\tilde{u}_{egr}) \tag{58}$$

is modeled as [2]

$$f_{egr}(\tilde{u}_{egr}) = b_{egr1}(1 - \cos(\min(a_{egr1}\, \tilde{u}_{egr} + a_{egr2}, \pi))) + b_{egr2} \tag{59}$$

where

$$b_{egr2} = -b_{egr1}(1 - \cos(\min(a_{egr2}, \pi))) \tag{60}$$

This function is plotted in Fig. 8. The signal $\tilde{u}_{egr}$ describes the EGR actuator dynamics. The EGR-valve is open when $\tilde{u}_{egr} = 100\%$ and closed when $\tilde{u}_{egr} = 0\%$.

Tuning parameters

- Π_{egropt}: optimal value of Π_{egr} for maximum value of the function Ψ_{egr} in (55)
- b_{egr1}, a_{egr1}, and a_{egr2}: coefficients in the function for the effective area

Initialization method

The tuning parameters above are initialized by solving a separable non-linear least-squares problem, see [3] for details about the solution method. The non-linear part of this problem minimizes $(W_{egr} - W_{egr,meas})^2$ with Π_{egropt}, a_{egr1}, and a_{egr2} as the optimization variables. In each iteration in the non-linear least-squares solver, the values for b_{egr1} is set to be the solution of a linear least-squares problem that minimizes $(W_{egr} - W_{egr,meas})^2$ for the current values of Π_{egropt}, a_{egr1}, and a_{egr2}. The variable W_{egr} is described by the model (53) and $W_{egr,meas}$ is calculated from measurements as $W_{egr,meas} = W_{ei} - W_c$ where W_{ei} is described by the model (37). Stationary measurements are used as inputs to the model. The result of the initialization is shown in Fig. 8 and 9 showing that the model describes different variables in the EGR-valve well. Fig. 9 also shows a validation of the EGR mass flow model. Both the tuning and the validation give a mean absolute error of 2.4 %. The parameters are then tuned according to the method in Sec. 7.1.

5.2 EGR-valve actuator

The EGR-valve actuator dynamics is modeled as a second order system with an overshoot and a time delay. This model consist of a subtraction between two first order systems with different gains and time constants according to

$$\tilde{u}_{egr} = K_{egr}\, \tilde{u}_{egr1} - (K_{egr} - 1)\tilde{u}_{egr2} \tag{61}$$

$$\frac{d}{dt}\, \tilde{u}_{egr1} = \frac{1}{\tau_{egr1}}(u_{egr}(t - \tau_{degr}) - \tilde{u}_{egr1}) \tag{62}$$

$$\frac{d}{dt}\, \tilde{u}_{egr2} = \frac{1}{\tau_{egr2}}(u_{egr}(t - \tau_{degr}) - \tilde{u}_{egr2}) \tag{63}$$

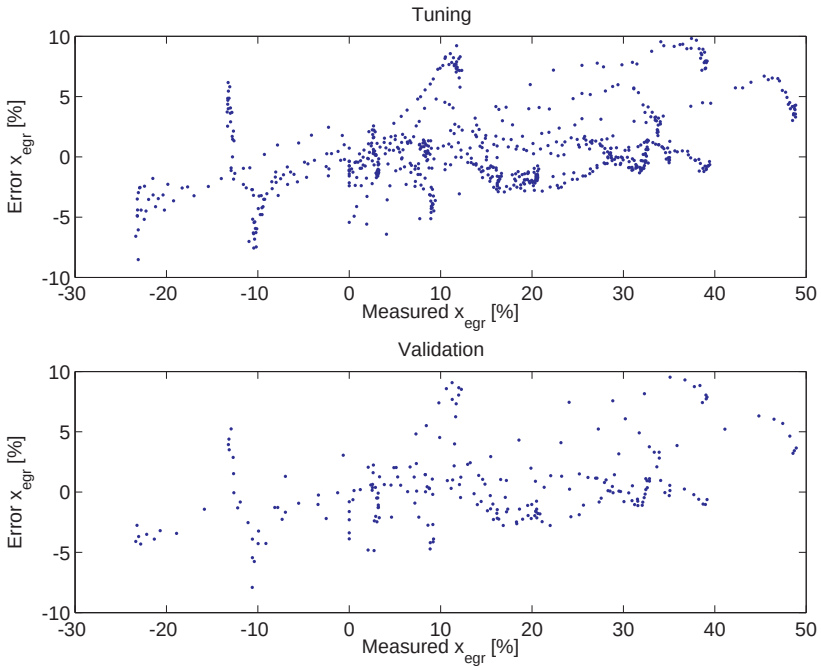

Figure 9: Error between modeled EGR fraction $x_{egr} = W_{egr}/(\max(W_{egr}, 0) + W_c)$ and calculated EGR fraction from measurements $x_{egr,meas} = (W_{ei} - W_c)/(\max(W_{ei} - W_c, 0) + W_c)$ for the tuning and validation data. Both the tuning and the validation give a mean absolute error of 2.4 %.

Tuning parameters

- τ_{egr1}, τ_{egr2}: time constants for the two different first order systems
- τ_{degr}: time delay
- K_{egr}: a parameter that affects the size of the overshoot

Tuning method

The values of the tuning parameters above are the same as for the EGR actuator model in [25].

6 Turbocharger

The turbocharger consists of a turbo inertia model, a turbine model, a VGT actuator model, and a compressor model.

6.1 Turbo inertia

For the turbo speed ω_t, Newton's second law gives

$$\frac{d}{dt}\omega_t = \frac{P_t\,\eta_m - P_c}{J_t\,\omega_t} \tag{64}$$

where J_t is the inertia, P_t is the power delivered by the turbine, P_c is the power required to drive the compressor, and η_m is the mechanical efficiency in the turbocharger.

Tuning parameter

- J_t: turbo inertia

Tuning method

The tuning parameter J_t is determined using least squares optimization for the complete model and using the first data set in Sec. 1.4.2, see Sec. 7.1 for more details.

6.2 Turbine

The turbine model consists of sub-models for the total turbine efficiency and the turbine mass flow, which also includes the VGT actuator as a sub-model.

6.2.1 Turbine efficiency

One way to model the power P_t is to use the turbine efficiency η_t, which is defined as [15]

$$\eta_t = \frac{P_t}{P_{t,s}} = \frac{T_{em} - T_t}{T_{em}(1 - \Pi_t^{1-1/\gamma_e})} \tag{65}$$

where T_t is the temperature after the turbine, Π_t is the pressure ratio

$$\Pi_t = \frac{p_t}{p_{em}} \tag{66}$$

and $P_{t,s}$ is the power from the isentropic process

$$P_{t,s} = W_t \, c_{pe} \, T_{em} \left(1 - \Pi_t^{1-1/\gamma_e}\right) \tag{67}$$

where W_t is the turbine mass flow. The pressure p_t is lower than the ambient pressure due to that there is a fan after the turbine and it is assumed that p_t is constant.

In (65) it is assumed that there are no heat losses in the turbine, i.e. it is assumed that there are no temperature drops between the temperatures T_{em} and T_t that is due to heat losses. This assumption leads to errors in η_t if (65) is used to calculate η_t from measurements. One way to improve this model is to model these temperature drops, but it is difficult to tune these models since there exists no measurements of these temperature drops. Another way to improve the model, that is frequently used in the literature [9], is to use another efficiency that are approximatively equal to η_t. This approximation utilizes that

$$P_t \, \eta_m = P_c \tag{68}$$

at steady state according to (64). Consequently, $P_t \approx P_c$ at steady state. Using this approximation in (65), another efficiency η_{tm} is obtained

$$\eta_{tm} = \frac{P_c}{P_{t,s}} = \frac{W_c \, c_{pa}(T_c - T_{bc})}{W_t \, c_{pe} \, T_{em} \left(1 - \Pi_t^{1-1/\gamma_e}\right)} \tag{69}$$

where T_c is the temperature after the compressor and W_c is the compressor mass flow. The temperature T_{em} in (69) introduces less errors compared to the temperature difference $T_{em} - T_t$ in (65) due to that the absolute value of T_{em} is larger than the absolute value of $T_{em} - T_t$. Consequently, (69) introduces less errors compared to (65) since (69) does not consist of $T_{em} - T_t$. The temperatures T_c and T_{amb} are low and they introduce less errors compared to T_{em} and T_t since the heat losses in the compressor are comparatively small. Another advantage of using (69) is that the individual variables P_t and η_m in (64) do not have to be modeled. Instead, the product $P_t\,\eta_m$ is modeled using (68) and (69)

$$P_t\,\eta_m = \eta_{tm}\,P_{t,s} = \eta_{tm}\,W_t\,c_{pe}\,T_{em}\left(1 - \Pi_t^{1-1/\gamma_e}\right) \tag{70}$$

Measurements show that η_{tm} depends on the blade speed ratio BSR, the turbo speed ω_t, and the VGT actuator position $\tilde{u}_{vgt}$. Therefore, η_{tm} is modeled using a product of three efficiencies

$$\eta_{tm} = \eta_{tm,BSR}(BSR) \cdot \eta_{tm,\omega_t}(\omega_t) \cdot \eta_{tm,\tilde{u}_{vgt}}(\tilde{u}_{vgt}) \tag{71}$$

The first efficiency $\eta_{BSR}(BSR)$ is modeled as a parabolic function [27] with a square on the input BSR (see Fig. 10 where $\eta_{tm,BSR}$ is plotted as function of BSR)

$$\eta_{tm,BSR}(BSR) = 1 - b_{BSR}\,(BSR^2 - BSR_{opt}^2)^2 \tag{72}$$

where the blade speed ratio BSR is the quotient of the turbine blade tip speed and the speed which a gas reaches when expanded isentropically at the given pressure ratio Π_t

$$BSR = \frac{R_t\,\omega_t}{\sqrt{2\,c_{pe}\,T_{em}\left(1 - \Pi_t^{1-1/\gamma_e}\right)}} \tag{73}$$

where R_t is the turbine blade radius.

The second efficiency $\eta_{tm,\omega_t}(\omega_t)$ is used in order to consider mechanical losses and it is modeled as two linear functions at two different regions (see Fig. 10 where η_{tm,ω_t} is plotted as function of ω_t)

$$\eta_{tm,\omega_t}(\omega_t) = \begin{cases} 1 - b_{\omega t1}\,\omega_t & \text{if } \omega_t \le \omega_{t,lim} \\ 1 - b_{\omega t1}\,\omega_{t,lim} - b_{\omega t2}(\omega_t - \omega_{t,lim}) & \text{if } \omega_t > \omega_{t,lim} \end{cases} \tag{74}$$

The third efficiency $\eta_{tm,\tilde{u}_{vgt}}(\tilde{u}_{vgt})$ is modeled as 3:rd order polynomial (see Fig. 10 where $\eta_{tm,\tilde{u}_{vgt}}$ is plotted as function of u_{vgt})

$$\eta_{tm,\tilde{u}_{vgt}}(\tilde{u}_{vgt}) = b_{vgt1}\,\tilde{u}_{vgt}^3 + b_{vgt2}\,\tilde{u}_{vgt}^2 + b_{vgt3}\,\tilde{u}_{vgt} + b_{vgt4} \tag{75}$$

Tuning parameters

- b_{BSR} and BSR_{opt}: parameters in the efficiency model (72)
- $b_{\omega t1}$, $b_{\omega t2}$, and $\omega_{t,lim}$: parameters in the efficiency model (74)
- b_{vgt1}, b_{vgt2}, b_{vgt3}, and b_{vgt4}: parameters in the efficiency model (75)
- p_t: Pressure after the turbine

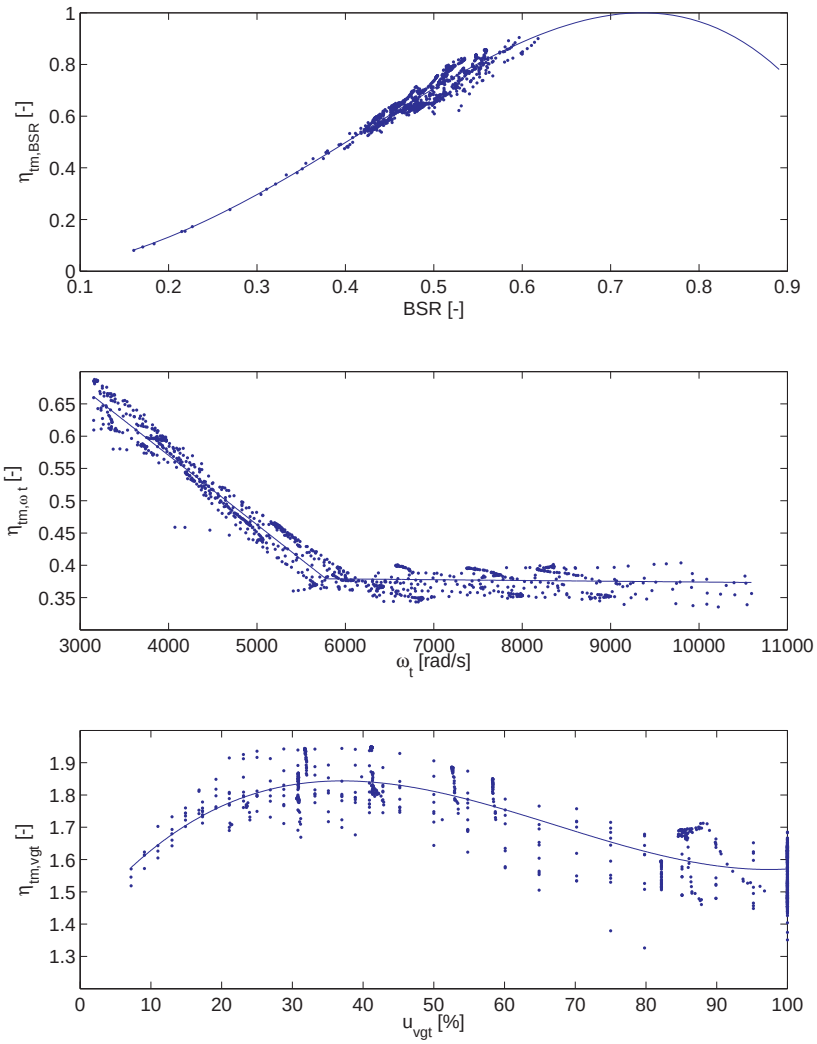

Figure 10: Comparison of calculated points from measurements and three sub-models for the turbine efficiency η_{tm} at steady state showing how different variables in the sub-models depend on each other. Note that this is not a validation of the sub-models since the calculated points for the sub-models depend on the model tuning. **Top:** The line shows the efficiency $\eta_{tm,BSR}$ (72) as function of BSR. The data points are calculated by solving (71) for $\eta_{tm,BSR}$. **Middle:** The line shows the efficiency η_{tm,ω_t} (74) as function of ω_t. The data points are calculated by solving (71) for η_{tm,ω_t}. **Bottom:** The line shows the efficiency $\eta_{tm,\tilde{u}_{vgt}}$ (75) as function of u_{vgt}. The data points are calculated by solving (71) for $\eta_{tm,\tilde{u}_{vgt}}$.

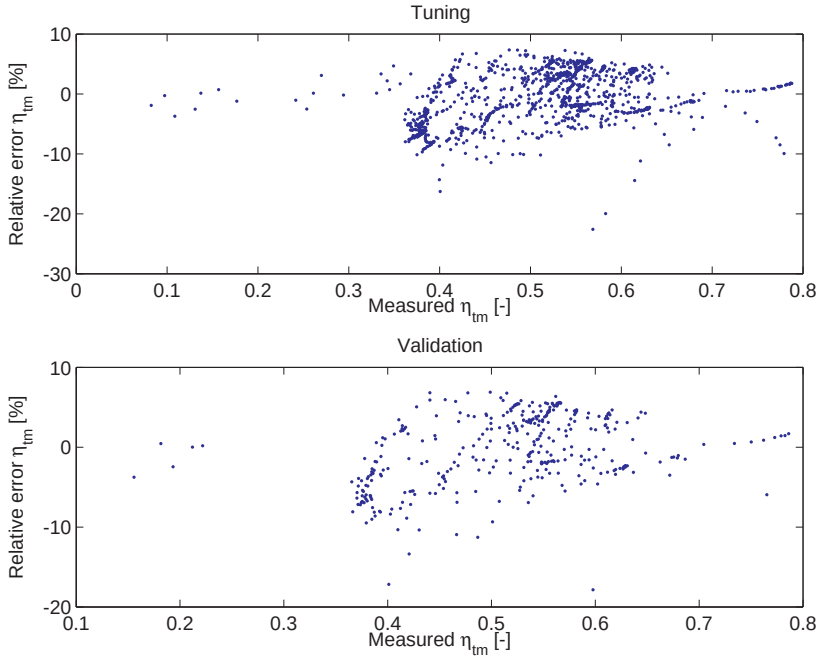

Figure 11: Relative error between the modeled and measured turbine efficiency η_{tm}. Both the tuning and the validation data give a mean absolute relative error of 3.7 %.

Tuning method for p_t

The parameter p_t is determined as the minimum value of p_{em} for the stationary tuning data.

Initialization method for the parameters above except p_t

The tuning parameters above except p_t are initialized by solving a separable non-linear least-squares problem, see [3] for details about the solution method. The non-linear part of this problem minimizes $(\eta_{tm} - \eta_{tm,meas})^2$ with b_{BSR}, BSR_{opt}, $b_{\omega t1}$, $b_{\omega t2}$, and $\omega_{t,lim}$ as the optimization variables. In each iteration in the non-linear least-squares solver, the values for b_{vgt1}, b_{vgt2}, b_{vgt3}, and b_{vgt4} are set to be the solution of a linear least-squares problem that minimizes $(\eta_{tm} - \eta_{tm,meas})^2$ for the current values of b_{BSR}, BSR_{opt}, $b_{\omega t1}$, $b_{\omega t2}$, and $\omega_{t,lim}$. The efficiency η_{tm} is described by the model (71) and $\eta_{tm,meas}$ is calculated from measurements using (69). Stationary measurements are used as inputs to the model. The result of the initialization and the validation are shown in Fig. 11 which shows that the model describes the total turbine efficiency well. Both the tuning and the validation data give a mean absolute relative error of 3.7 %. The parameters except p_t are then tuned according to the method in Sec. 7.1.

6.2.2 Turbine mass flow

The turbine mass flow W_t is modeled using the corrected mass flow in order to consider density variations in the mass flow [15, 27]

$$\frac{W_t \sqrt{T_{em} R_e}}{p_{em}} = A_{vgtmax} f_{\Pi t}(\Pi_t) f_{\omega t}(\omega_{t,corr}) f_{vgt}(\tilde{u}_{vgt}) \tag{76}$$

where A_{vgtmax} is the maximum area in the turbine that the gas flows through. Measurements show that the corrected mass flow depends on the pressure ratio Π_t, the corrected turbocharger speed $\omega_{t,corr}$ and the VGT actuator signal $\tilde{u}_{vgt}$. As the pressure ratio decreases, the corrected mass flow increases until the gas reaches the sonic condition and the flow is choked. This behavior can be described by a choking function

$$f_{\Pi t}(\Pi_t) = \sqrt{1 - \Pi_t^{K_t}} \tag{77}$$

which is not based on the physics of the turbine, but it gives good agreement with measurements using few parameters [10], see Fig. 12 where $f_{\Pi t}$ is plotted as function of Π_t. The function $f_{\omega t}(\omega_{t,corr})$ is modeled as a parabolic function, see Fig. 12 where $f_{\omega t}$ is plotted as function of $\omega_{t,corr}$

$$f_{\omega t}(\omega_{t,corr}) = 1 - c_{\omega t} \left(\omega_{t,corr} - \omega_{t,corropt}\right)^2 \tag{78}$$

where

$$\omega_{t,corr} = \frac{\omega_t}{100\sqrt{T_{em}}} \tag{79}$$

When the VGT control signal u_{vgt} increases, the effective area increases and hence also the flow increases. Due to the geometry in the turbine, the change in effective area is large when the VGT control signal is small. This behavior can be described by a part of an ellipse (see Fig. 12 where f_{vgt} is plotted as function of u_{vgt})

$$\left(\frac{f_{vgt}(\tilde{u}_{vgt}) - c_{f2}}{c_{f1}}\right)^2 + \left(\frac{\tilde{u}_{vgt} - c_{vgt2}}{c_{vgt1}}\right)^2 = 1 \tag{80}$$

where f_{vgt} is the effective area ratio function and $\tilde{u}_{vgt}$ describes the VGT actuator dynamics.

The flow can now be modeled by solving (76) for W_t giving

$$W_t = \frac{A_{vgtmax}\, p_{em}\, f_{\Pi t}(\Pi_t)\, f_{\omega t}(\omega_{t,corr})\, f_{vgt}(\tilde{u}_{vgt})}{\sqrt{T_{em} R_e}} \tag{81}$$

and solving (80) for f_{vgt} giving

$$f_{vgt}(\tilde{u}_{vgt}) = c_{f2} + c_{f1}\sqrt{\max(0, 1 - \left(\frac{\tilde{u}_{vgt} - c_{vgt2}}{c_{vgt1}}\right)^2)} \tag{82}$$

Tuning parameters

- K_t: exponent in the choking function for the turbine flow
- $c_{\omega t}$ and $\omega_{t,corropt}$: parameters in the function $f_{\omega t}$ (78)
- c_{f1}, c_{f2}, c_{vgt1}, c_{vgt2}: parameters in the ellipse for the effective area ratio function

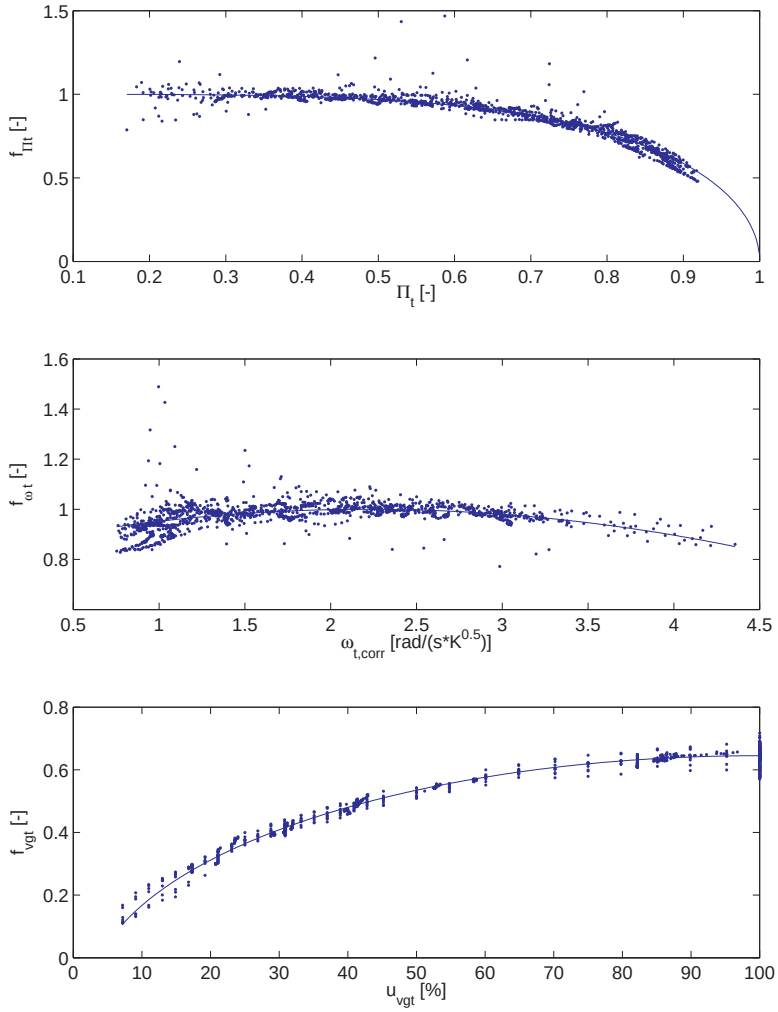

Figure 12: Comparison of calculated points from measurements and three sub-models for the turbine mass flow at steady state showing how different variables in the sub-models depend on each other. Note that this is not a validation of the sub-models since the calculated points for the sub-models depend on the model tuning. **Top:** The line shows the choking function $f_{\Pi t}$ (77) as function of the pressure ratio Π_t. The data points are calculated by solving (76) for $f_{\Pi t}$. **Middle:** The line shows the function $f_{\omega t}$ (78) as function of the corrected turbocharger speed $\omega_{t,corr}$. The data points are calculated by solving (76) for $f_{\omega t}$. **Bottom:** The line shows the effective area ratio function f_{vgt} (82) as function of the control signal u_{vgt}. The data points are calculated by solving (76) for f_{vgt}.

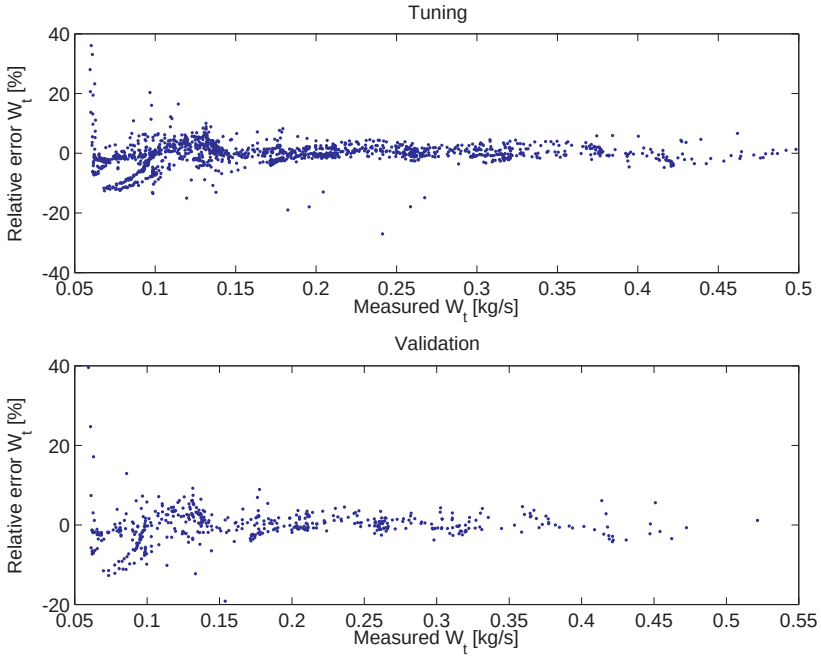

Figure 13: Relative error between the modeled and measured turbine mass flow W_t for the tuning and validation data. The tuning and the validation data give a mean absolute relative error of 2.8 % respectively 2.7 %.

Initialization method

The tuning parameters above are initialized by solving a non-linear least-squares problem that minimizes $(W_t - W_{t,meas})^2$ with the tuning parameters as the optimization variables. The flow W_t is described by the model (81), (82), and (77), and $W_{t,meas}$ is calculated from measurements as $W_{t,meas} = W_c + W_f$, where W_f is calculated using (39). Stationary measurements are used as inputs to the model. The result of the initialization and the validation are shown in Fig. 13 which shows that the model describes the turbine mass flow well. The tuning and the validation data give a mean absolute relative error of 2.8 % respectively 2.7 %. The parameters are then tuned according to the method in Sec. 7.1.

6.2.3 VGT actuator

The VGT actuator dynamics is modeled as a first order system with a time delay according to

$$\frac{d}{dt}\,\tilde{u}_{vgt} = \frac{1}{\tau_{vgt}}(u_{vgt}(t - \tau_{dvgt}) - \tilde{u}_{vgt}) \tag{83}$$

Tuning parameters

- τ_{vgt}: time constant

- τ_{dvgt}: time delay

Tuning method

The values of the tuning parameters above are the same as for the VGT actuator model in [25].

6.3 Compressor

The compressor model consists of sub-models for the compressor efficiency and the compressor mass flow.

6.3.1 Compressor efficiency

The compressor power P_c is modeled using the compressor efficiency η_c, which is defined as [15]

$$\eta_c = \frac{P_{c,s}}{P_c} = \frac{T_{bc}\left(\Pi_c^{1-1/\gamma_a} - 1\right)}{T_c - T_{bc}} \tag{84}$$

where T_c is the temperature after the compressor, Π_c is the pressure ratio

$$\Pi_c = \frac{p_{ic}}{p_{bc}} \tag{85}$$

where p_{bc} is assumed to be equal to the ambient pressure p_{amb}, and $P_{c,s}$ is the power from the isentropic process

$$P_{c,s} = W_c\, c_{pa}\, T_{bc}\left(\Pi_c^{1-1/\gamma_a} - 1\right) \tag{86}$$

where W_c is the compressor mass flow. The power P_c is modeled by solving (84) for P_c and using (86)

$$P_c = \frac{P_{c,s}}{\eta_c} = \frac{W_c\, c_{pa}\, T_{bc}}{\eta_c}\left(\Pi_c^{1-1/\gamma_a} - 1\right) \tag{87}$$

The efficiency is modeled based on the proposed model in [13] where the corrected mass flow $W_{c,corr}$ and Π_c are used as inputs. To improve the agreement with measured data, the ellipses in [13] are replaced by a product of efficiencies similar to [9] according to

$$\eta_c(W_{c,corr}, \Pi_c) = \eta_{c,W}(W_{c,corr}, \Pi_c) \cdot \eta_{c,\Pi}(\Pi_c) \tag{88}$$

$$\eta_{c,W}(W_{c,corr}, \Pi_c) = 1 - a_{W3}(W_{c,corr} - (a_{W1} + a_{W2}\,\Pi_c))^2 \tag{89}$$

$$\eta_{c,\Pi}(\Pi_c) = \begin{cases} a_{\Pi1}\,\Pi_c^2 + a_{\Pi2}\,\Pi_c + a_{\Pi3} & \text{if } \Pi_c < \Pi_{c,lim} \\ a_{\Pi4}\,\Pi_c^2 + a_{\Pi5}\,\Pi_c + a_{\Pi6} & \text{if } \Pi_c \geq \Pi_{c,lim} \end{cases} \tag{90}$$

where

$$a_{\Pi6} = \Pi_{c,lim}^2(a_{\Pi1} - a_{\Pi4}) + \Pi_{c,lim}(a_{\Pi2} - a_{\Pi5}) + a_{\Pi3} \tag{91}$$

and

$$W_{c,corr} = \frac{W_c\sqrt{(T_{bc}/T_{ref})}}{(p_{bc}/p_{ref})} \tag{92}$$

This model is plotted as a map in Fig. 17.

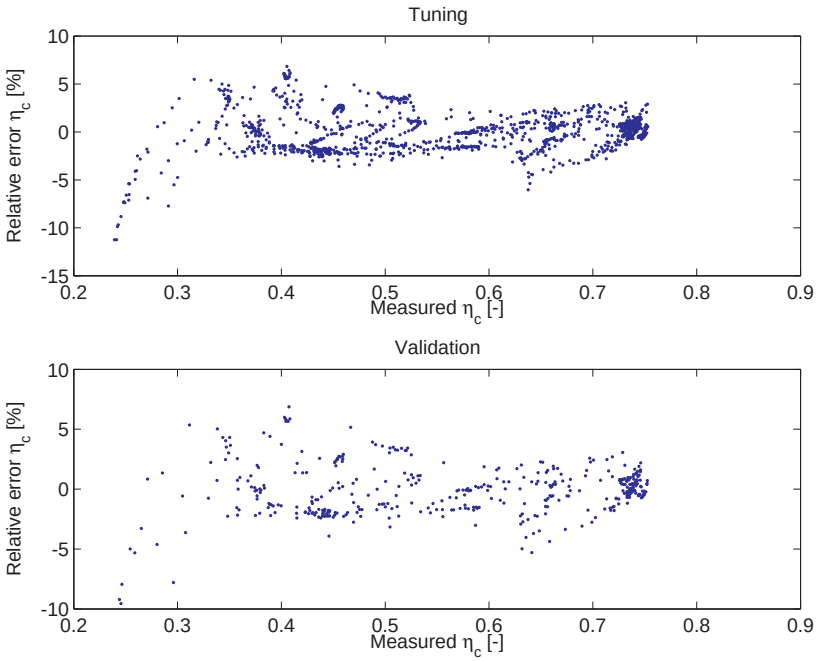

Figure 14: Relative error between the modeled and measured compressor efficiency η_c for the tuning and validation data. Both the tuning and the validation data give a mean absolute relative error of 1.6 %.

Tuning model parameters

- a_{W1}, a_{W2}, and a_{W3}: parameters in the efficiency model (89)
- $a_{\Pi 1}$, $a_{\Pi 2}$, $a_{\Pi 3}$, $a_{\Pi 4}$, and $a_{\Pi 5}$: parameters in the efficiency model (90)
- $\Pi_{c,lim}$: Pressure ratio limit in the efficiency model (90)

Initialization method

The tuning parameters above are initialized by solving a separable non-linear least-squares problem, see [3] for details about the solution method. The non-linear part of this problem minimizes $(\eta_c - \eta_{c,meas})^2$ with a_{W1}, a_{W2}, a_{W3}, $a_{\Pi 4}$, $a_{\Pi 5}$, and $\Pi_{c,lim}$ as the optimization variables. In each iteration in the non-linear least-squares solver, the values for $a_{\Pi 1}$, $a_{\Pi 2}$, and $a_{\Pi 3}$ are set to be the solution of a linear least-squares problem that minimizes $(\eta_c - \eta_{c,meas})^2$ for the current values of a_{W1}, a_{W2}, a_{W3}, $a_{\Pi 4}$, $a_{\Pi 5}$, and $\Pi_{c,lim}$. The efficiency η_c is described by the model (88) to (92) and $\eta_{c,meas}$ is calculated from measurements using (84). Stationary measurements are used as inputs to the model. The result of the initialization and the validation are shown in Fig. 14 which shows that the model describes the compressor efficiency well. Both the tuning and the validation data give a mean absolute relative error of 1.6 %. The parameters are then tuned according to the method in Sec. 7.1.

6.3.2 Compressor mass flow

The mass flow W_c through the compressor is modeled using two dimensionless variables. The first variable is the energy transfer coefficient [6]

$$\Psi_c = \frac{2\, c_{pa}\, T_{bc} \left(\Pi_c^{1-1/\gamma_a} - 1 \right)}{R_c^2\, \omega_t^2} \tag{93}$$

which is the quotient of the isentropic kinetic energy of the gas at the given pressure ratio Π_c and the kinetic energy of the compressor blade tip where R_c is compressor blade radius. The second variable is the volumetric flow coefficient [6]

$$\Phi_c = \frac{W_c/\rho_{bc}}{\pi\, R_c^3\, \omega_t} = \frac{R_a\, T_{bc}}{p_{bc}\, \pi\, R_c^3\, \omega_t} W_c \tag{94}$$

which is the quotient of volume flow rate of air into the compressor and the rate at which volume is displaced by the compressor blade where ρ_{bc} is the density of the air before the compressor. The relation between Ψ_c and Φ_c can be described as follows [17, 9]

$$\Phi_c = \frac{k_{c1} - k_{c3}\, \Psi_c}{k_{c2} - \Psi_c} \tag{95}$$

$$k_{ci} = k_{ci1}\, (\min(Ma, Ma_{max}))^2 + k_{ci2}\, \min(Ma, Ma_{max}) + k_{ci3}, \quad i = 1, \ldots, 3 \tag{96}$$

$$Ma = \frac{R_c\, \omega_t}{\sqrt{\gamma_a\, R_a\, T_{bc}}} \tag{97}$$

where Ma is the Mach number at the ring orifice of the compressor. This relation is shown in Fig. 15 where Φ_c is plotted as function of Ψ_c.

The mass flow is modeled by solving (94) for W_c.

$$W_c = \frac{p_{bc}\, \pi\, R_c^3\, \omega_t}{R_a\, T_{bc}} \Phi_c \tag{98}$$

Tuning model parameters

- k_{ci1}, k_{ci2}, k_{ci3}, for $i = 1, \ldots, 3$: coefficients in the polynomial functions (96)
- Ma_{max}: maximum Mach number

Tuning method for Ma_{max}

The tuning parameter Ma_{max} is determined as $Ma_{max} = \max(Ma_{meas})$ where Ma_{meas} is calculated from measurements using (97).

Initialization method k_{ci1}, k_{ci2}, and k_{ci3}

The tuning parameters k_{ci1}, k_{ci2}, and k_{ci3} for $i = 1, \ldots, 3$ are initialized by solving a separable non-linear least-squares problem, see [3] for details about the solution method. The non-linear part of this problem minimizes $(\Phi_c - \Phi_{c,meas})^2$

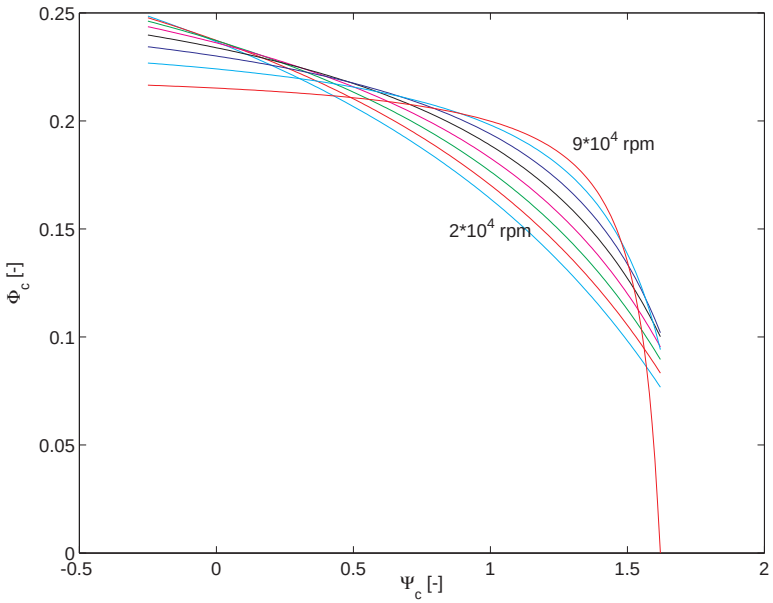

Figure 15: The lines show the volumetric flow coefficient Φ_c (95) as function of energy transfer coefficient Ψ_c at 8 different turbo speeds between $2 \cdot 10^4$ rpm and $9 \cdot 10^4$ rpm.

with k_{c2j} for $j = 1, \ldots, 3$ as the optimization variables. In each iteration in the non-linear least-squares solver, the values for k_{c1j} and k_{c3j} for $j = 1, \ldots, 3$ are set to be the solution of a linear least-squares problem that minimizes $(\Phi_c - \Phi_{c,meas})^2$ for the current values of k_{c2j} for $j = 1, \ldots, 3$. The volumetric flow coefficient Φ_c is described by the model (95)-(97) and $\Phi_{c,meas}$ is calculated from measurements using (94). Stationary measurements are used as inputs to the model. The result of the initialization and the validation are shown in Fig. 16 which shows that the model describes the compressor mass flow well. Both the tuning and the validation data give a mean absolute relative error of 1.7 %. The parameters k_{ci1}, k_{ci2}, and k_{ci3} are then tuned according to the method in Sec. 7.1.

6.3.3 Compressor map

Compressor performance is usually presented in terms of a map with Π_c and $W_{c,corr}$ on the axes showing lines of constant efficiency and constant turbo speed. This is shown in Fig. 17 which has approximatively the same characteristics as Fig. 2.10 in [27]. Consequently, the proposed model of the compressor efficiency (88) and the compressor flow (98) has the expected behavior.

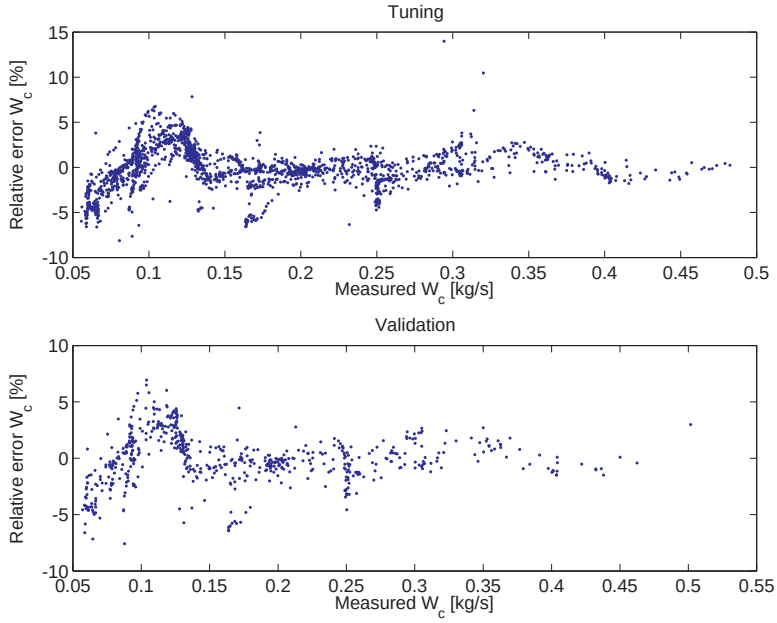

Figure 16: Relative error between the modeled and measured compressor mass flow W_c for the tuning and validation data. Both the tuning and the validation data give a mean absolute relative error of 1.7 %.

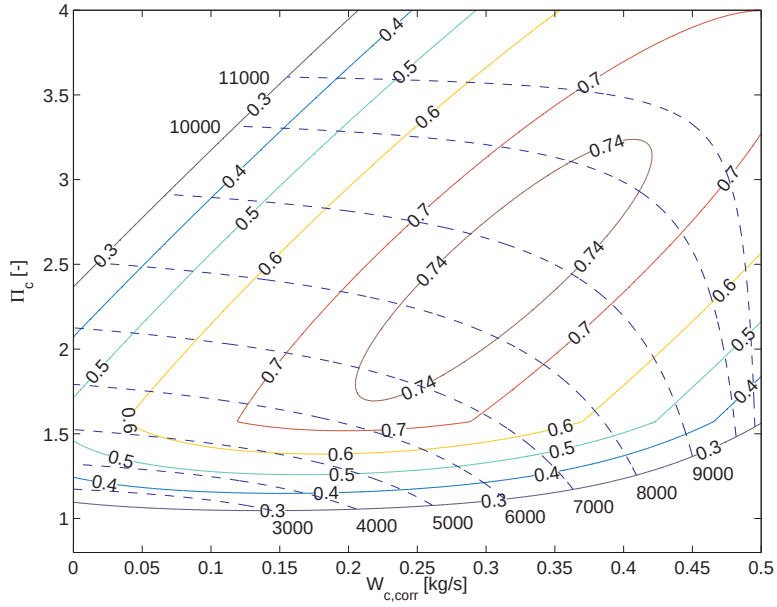

Figure 17: Compressor map with modeled efficiency lines (solid line) and modeled turbo speed lines (dashed line with turbo speed in rad/s). The turbo speed lines are described by the compressor flow model.

7 Model tuning and validation

One step in the development of a model that describes the system dynamics and the nonlinear effects is the tuning and validation. In Sec. 7.1 the model tuning is described, in Sec. 7.2 it investigated how the tuning affects the model quality of the sub-models and if the model captures the essential dynamic behaviors and nonlinear effects, and in Sec. 7.3 a validation of the complete model is performed using dynamic data. The data that is used in the tuning and validation are described in Sec. 1.4.

7.1 Tuning

As described in Sec. 1.5, the model parameters are estimated in four steps.

7.1.1 Initialization method

Firstly, parameters in static models are initialized automatically using least squares optimization of the sub-models and using 75% of the data from stationary measurements. The initialization methods for each parameter and the results are described in Sec. 4 to 6.

7.1.2 Parameters in static models

Secondly, the parameters in static models are finally estimated automatically using a least squares optimization that minimizes errors both in sub-models and in the complete model. This is an important step in the tuning method in order to reduce errors in the complete model. If only the first step above is used in the tuning method, the mean of all relative errors will become 5.7 %. However, if also the second step is used the mean of all relative errors will become 3.7 %. Consequently, it is important to use both the sub-models and the complete model in the optimization and not only the sub-models.

The least squares optimization problem is formulated as

$$\begin{aligned} &\min V(\theta) \\ &\text{s.t. } \theta_{min} \leq \theta \leq \theta_{max} \end{aligned} \tag{99}$$

where $V(\theta)$ is the cost function

$$\begin{aligned} V(\theta) = &\frac{1}{K}\sum_{k=1}^{K}\frac{\gamma_k^2}{L_k}\sum_{l=1}^{L_k}\left(\frac{y_k^{meas}[l]-y_k^{mod}[l]}{\max_i y_k^{meas}[i]}\right)^2 + \\ &\frac{1}{\beta\, N}\sum_{n=1}^{N}\frac{1}{M_n}\sum_{m=1}^{M_n}\left(\frac{z_n^{meas}[m]-z_n^{mod}[m]}{\max_i z_n^{meas}[i]}\right)^2 \end{aligned}$$

and θ are the static model parameters, and θ_{min} and θ_{max} are lower and upper bounds for the parameters.

The first row in the cost function minimizes errors between stationary measurements y_k^{meas} (75% of the data from stationary measurements in Sec. 1.4.1) and stationary simulations y_k^{mod} of the complete model. The second row minimizes errors between stationary measurements z_n^{meas} and stationary simulations

Table 3: The mean absolute relative errors and mean absolute errors between stationary tuning data and diesel engine model simulation and between stationary validation data and diesel engine model simulation. The model parameters are tuned according to the method in Sec. 7.1.

	Mean absolute relative errors [%]						Mean absolute errors	
	p_{im}	p_{em}	p_{ic}	W_c	ω_t	mean of all rel errors	x_{egr} [%]	T_{em} [K]
Tuning	2.8	3.0	2.8	4.2	5.7	3.7	1.2	14.7
Validation	3.6	3.0	3.5	4.5	7.4	4.4	1.8	15.1

z_n^{mod} of each sub-model. There are seven outputs in the simulation of the complete model

$$y_1 = p_{im}, \quad y_2 = p_{em}, \quad y_3 = p_{ic}, \quad y_4 = W_c,$$
$$y_5 = W_{egr}, \quad y_6 = n_t, \quad y_7 = T_{em}$$

and there are eight outputs in the simulation of each sub-model

$$z_1 = W_{th}, \quad z_2 = W_{ei}, \quad z_3 = T_{em}, \quad z_4 = W_{egr},$$
$$z_5 = \eta_{tm}, \quad z_6 = W_t, \quad z_7 = \eta_c, \quad z_8 = W_c$$

The signals z_n^{meas} and z_n^{mod} are calculated according to the initialization methods in Sec. 4 to 6. Further, K is the number of outputs in the simulation of the complete model with $K = 7$. The constant L_k is the number of operating points for the output y_k. The constant N is the number of outputs in the the simulation of each sub-model with $N = 8$ and M_n is the number of operating points for the output z_n.

Each term in the first row in the cost function is normalized with $K \cdot L_k \cdot \max_i y_k^{meas}[i]$ and each term in the second row is normalized with $N \cdot M_n \cdot \max_i z_n^{meas}[i]$ in order to penalize different outputs equally and to penalize simulations of the complete model and the sub-models equally. The parameters β and γ_k are tuning parameters in the optimization problem and they are set to

$$\beta = 4, \quad \gamma_5 = 2$$
$$\gamma_k = 1, \text{ for } k = 1, \ldots, 4, 6, 7$$

The optimization problem is solved using a standard Matlab non-linear least square solver and the parameters are initialized using the method in the first step above. The result of the optimization is shown in Tab. 3 showing that the mean of all relative errors is 3.7 % on the tuning data (75% of the data from stationary measurements) and 4.4 % on the validation data (25% of the data from stationary measurements).

7.1.3 Parameters in dynamic models

Thirdly, the actuator parameters for the intake throttle are estimated using least squares optimization for the actuator model and using the measurements from the first dynamic data set in Sec. 1.4.2 that only consist of steps in throttle

position, see Sec. 3.1 for more details. The parameters values for the EGR and VGT actuator models are set to be the same as the model in [25].

Fourthly, the control volumes in the intercooler, intake manifold, and exhaust manifold and the turbocharger inertia are estimated by solving the following least squares optimization problem

$$\begin{aligned} &\min V(\theta) \\ &\text{s.t. } \theta_{min} \leq \theta \leq \theta_{max} \end{aligned} \tag{100}$$

where $V(\theta)$ is the cost function

$$V(\theta) = \sum_{k=1}^{K} \sum_{l=1}^{L_k} \left(w_k^{meas,dyn}[l] - w_k^{mod,dyn}[l] \right)^2 \tag{101}$$

and θ are the control volumes and the turbocharger inertia, and θ_{min} and θ_{max} are lower and upper bounds for the parameters. The cost function minimizes errors between dynamic measurements $w_k^{meas,dyn}$ (the first dynamic data set in Sec. 1.4.2) and dynamic simulations $w_k^{mod,dyn}$ of the complete model. There are five outputs ($K = 5$) in the dynamic measurements and simulations

$$w_1 = p_{im}^{norm}, \quad w_2 = p_{em}^{norm}, \quad w_3 = p_c^{norm}, \quad w_4 = W_c^{norm}, \quad w_5 = n_t^{norm}$$

where each output and each step response is normalized so that the initial and final values for each step response are the same for both the measurements and the simulations, i.e. there are only dynamic errors in the outputs and no stationary errors. Further, L_k is the number of samples for the output w_k where both dynamic measurements and simulations are sampled with a frequency of 100 Hz.

7.2 Tuning results

The tuning results consist of an investigation of the change of errors in sub-models and a verification of essential system properties and time constants.

7.2.1 Change of errors in sub-models

The change of errors in the sub-models between the initialization step in Sec. 7.1.1 and the optimization step in Sec. 7.1.2 are calculated in Tab. 4. This table shows that the sub-models in the turbocharger (W_c, η_c, W_t, and η_{tm}) have the largest changes in errors. Consequently, the minimization of the errors in the complete model gives large increases in errors for the sub-models in the turbocharger.

7.2.2 Verification of essential system properties and time constants

The references [20], [19], and [25] show the essential system properties for the pressures and the flows in a diesel engine with VGT and EGR. Some of these properties are a non-minimum phase behavior in the intake manifold pressure and a non-minimum phase behavior, an overshoot, and a sign reversal in the compressor mass flow. The goal is to investigate if these system properties also exist in a diesel engine with intake throttle, VGT, and EGR, and if there are other system properties in this system. The goal is also to investigate if the

Table 4: Change of errors in sub-models after the optimization of the complete model in Sec. 7.1.2.

Sub-model	Error after initialization of sub-models (Sec. 7.1.1)	Error after optimization of the complete model (Sec. 7.1.2)	Relative change [%]
W_c	1.7 %	15.9 %	822
η_c	1.5 %	13.1 %	745
W_t	2.8 %	16.3 %	491
η_{tm}	3.7 %	10.0 %	172
W_{ei}	1.6 %	2.3 %	37
T_{em}	9.5 K	11.0 K	16
W_{th}	2.0 %	2.3 %	14
x_{egr}	2.4 %	2.4 %	-2

proposed model captures these system properties. This is investigated by using the first dynamic data in Sec. 1.4.2. Three different step responses from this data are shown in Fig. 18-20. Fig. 18 shows that the model captures the non-minimum phase behavior in the first step and the overshoot in the second step in the channel u_{vgt} to W_c. This figure also shows that the model captures that the DC-gain is negative in the first step and that the DC-gain is positive in the second step in the channel u_{vgt} to W_c. Consequently, there is a sign reversal in this channel. Fig. 18 also shows that the model captures the non-minimum phase behavior in the second step in the channel u_{vgt} to n_t. Fig. 19 shows that the model captures the non-minimum phase behavior in the channels u_{egr} to p_{ic} and u_{egr} to p_{im}. Fig. 20 shows that the model captures the non-minimum phase behavior in the channel u_{th} to p_{ic}. Further, Fig. 18-20 also show that the model captures the fast dynamics in the beginning of the responses and the slow dynamics in the end of the responses.

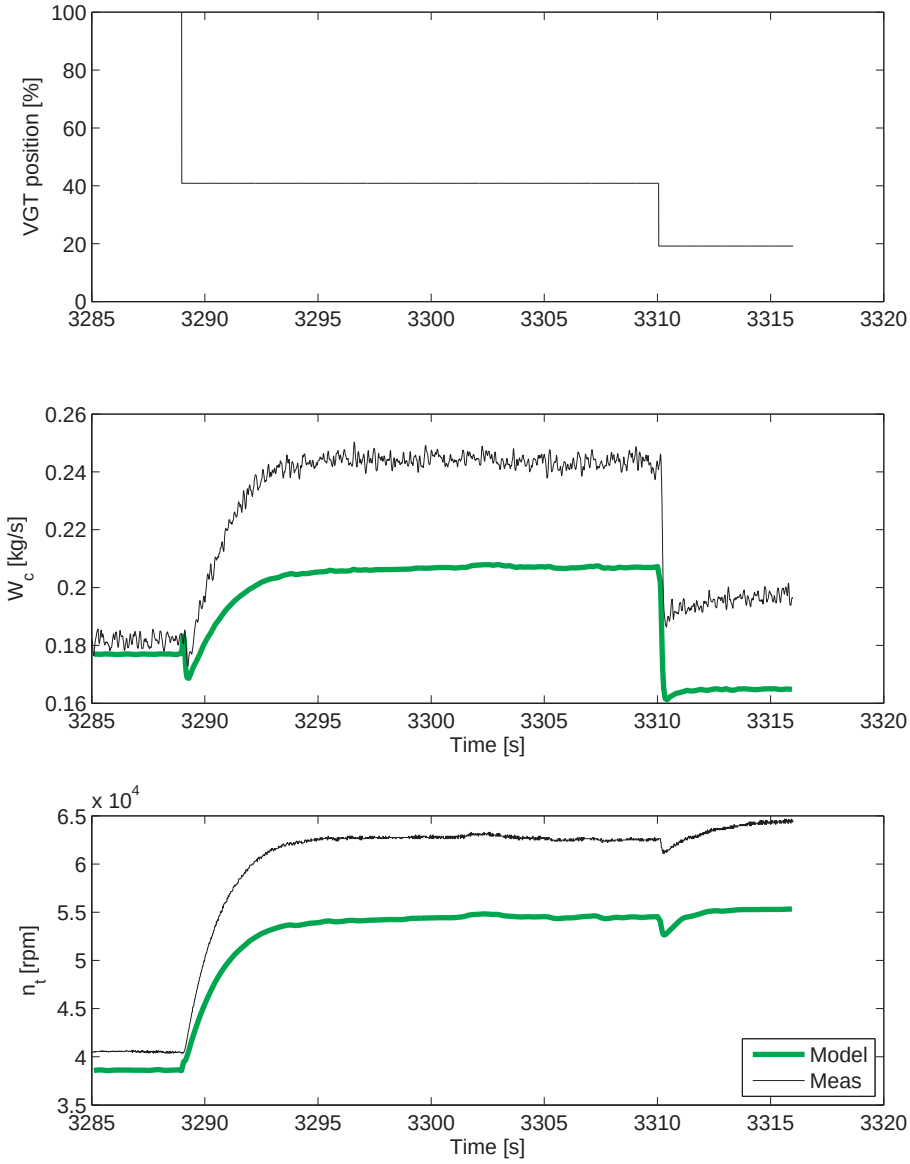

Figure 18: Comparison between diesel engine model simulation and dynamic tuning data showing that the model captures the non-minimum phase behavior, overshoot, and sign reversal in W_c, and the non-minimum phase behavior in n_t. Operating point: u_δ=67 mg/cycle, n_e=2000 rpm, u_{egr}=40 %, and u_{th}=100 %.

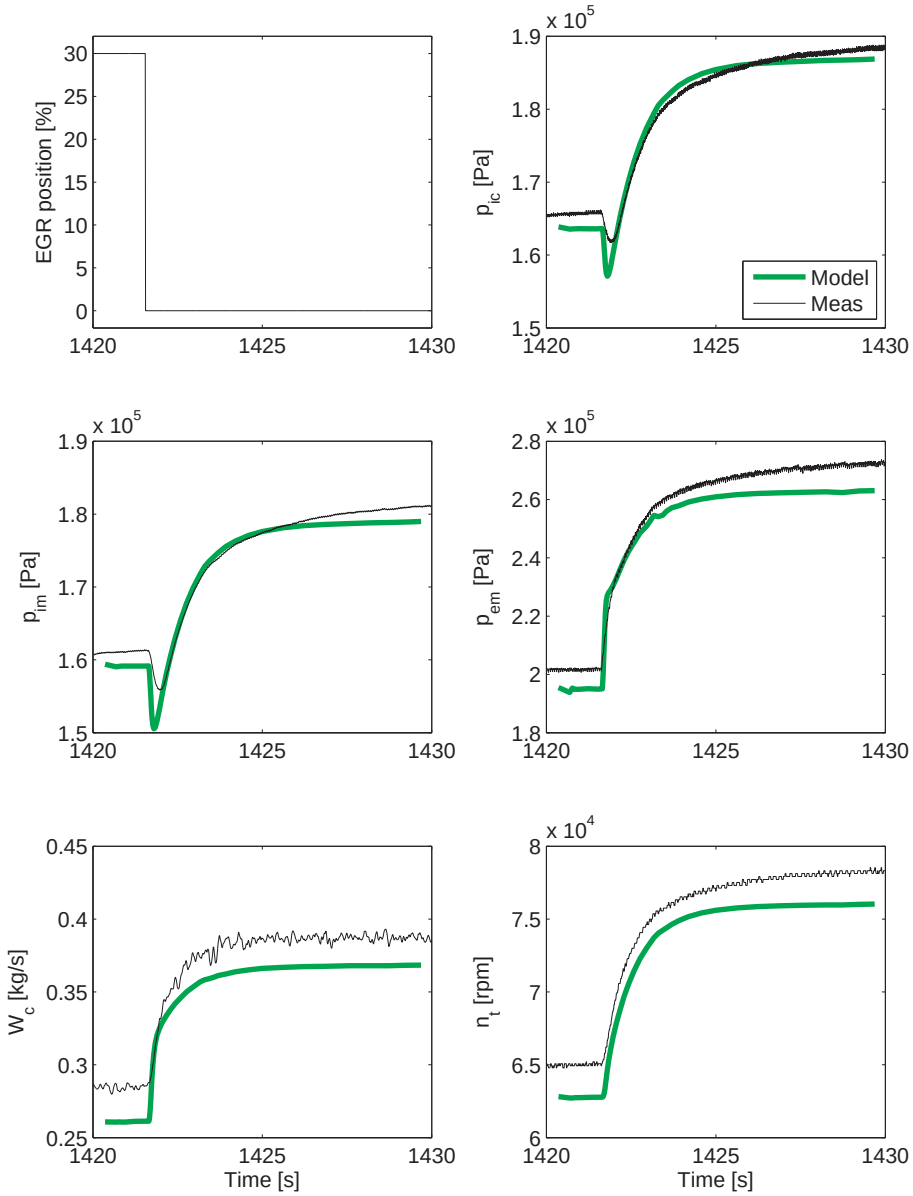

Figure 19: Comparison between diesel engine model simulation and dynamic tuning data showing that the model captures the non-minimum phase behavior in p_{ic} and p_{im}. Operating point: u_δ=147 mg/cycle, n_e=2000 rpm, u_{vgt}=88 %, and u_{th}=100 %.

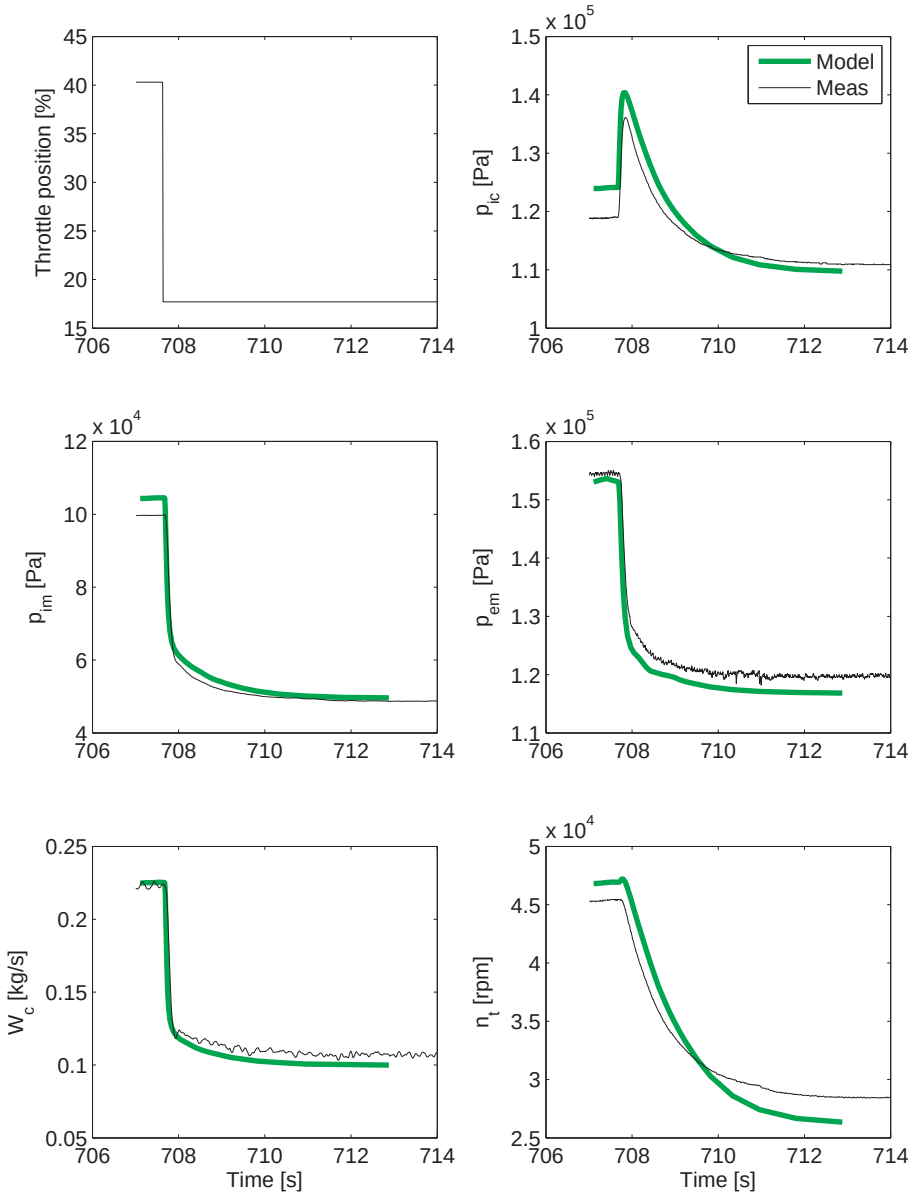

Figure 20: Comparison between diesel engine model simulation and dynamic tuning data showing that the model captures the non-minimum phase behavior in p_{ic}. Operating point: u_δ=58 mg/cycle, n_e=2000 rpm, u_{vgt}=100 %, and u_{egr}=0 %.

7.3 Validation

The complete model is validated both in stationary and dynamic conditions using the second data set in Sec. 1.4.2 that consists of measurements from the World Harmonized Transient Cycle (WHTC) [7]. The model is validated for the complete WHTC cycle in Sec. 7.3.1 and for some aggressive WHTC transients in Sec. 7.3.2.

7.3.1 Complete WHTC cycle

The proposed model is validated for the complete WHTC cycle in Tab. 5 showing that the mean value of all absolute relative errors for all measured outputs are equal to 7.4 %.

Table 5: The mean absolute relative errors [%] between dynamic validation data and diesel engine model simulation. The model parameters are tuned according to the method in Sec. 7.1.

p_{im}	p_{em}	p_{ic}	W_c	ω_t	mean of all rel errors
8.7	4.8	4.9	8.1	10.3	7.4

7.3.2 Aggressive WHTC transients

The proposed model is validated for some aggressive WHTC transients in Fig. 21-23. Fig. 21 shows the inputs and Fig. 22 and 23 compare the outputs showing that the model captures the dynamics and the stationary conditions in the measurements except at high fuel injections where the simulated outputs are higher than the measured outputs. Since the engine model will be used in a controller the steady state accuracy is less important since a controller will take care of steady state errors. However, in order to design a successful controller, it is important that the model captures the essential dynamic behaviors and nonlinear effects which is true for the proposed model according to this section and Sec. 7.2.2.

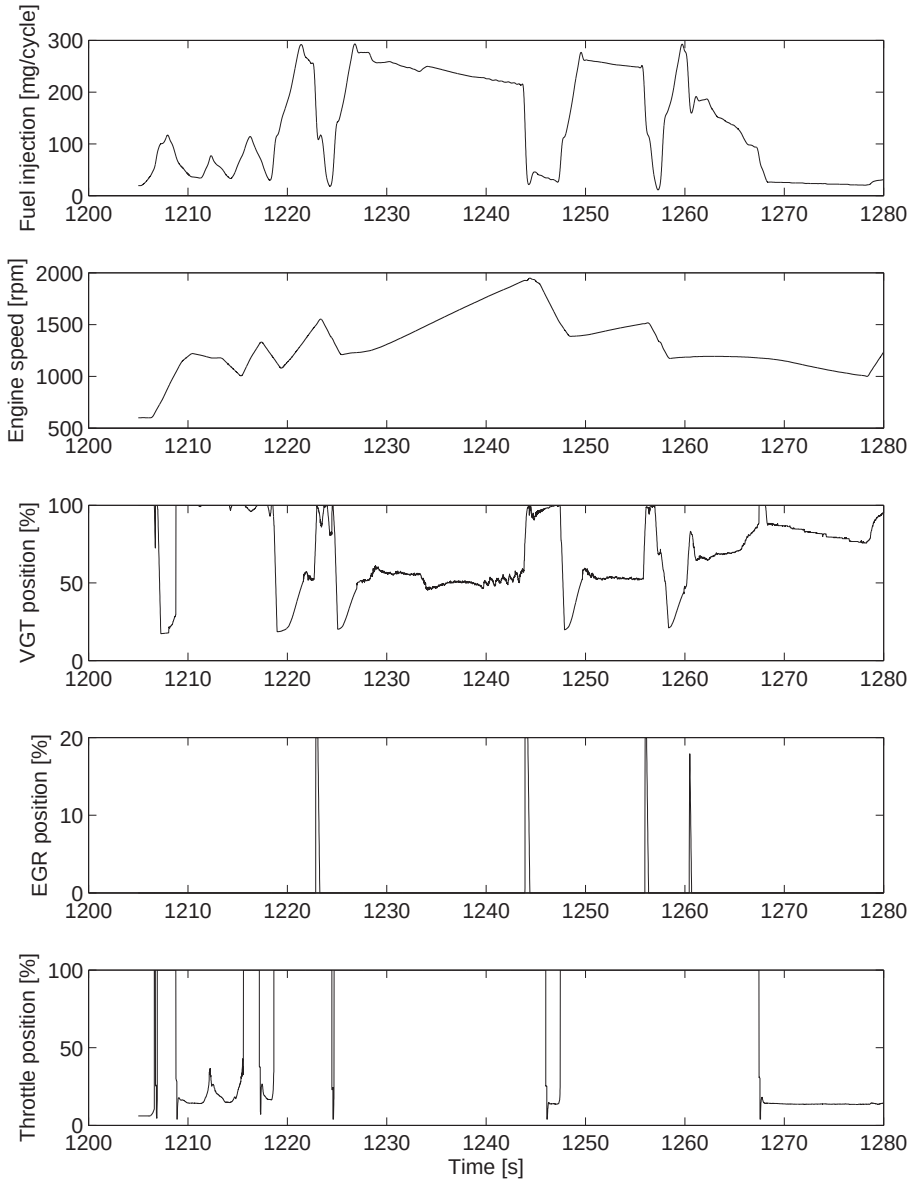

Figure 21: Inputs from the dynamic validation data for some aggressive WHTC transients.

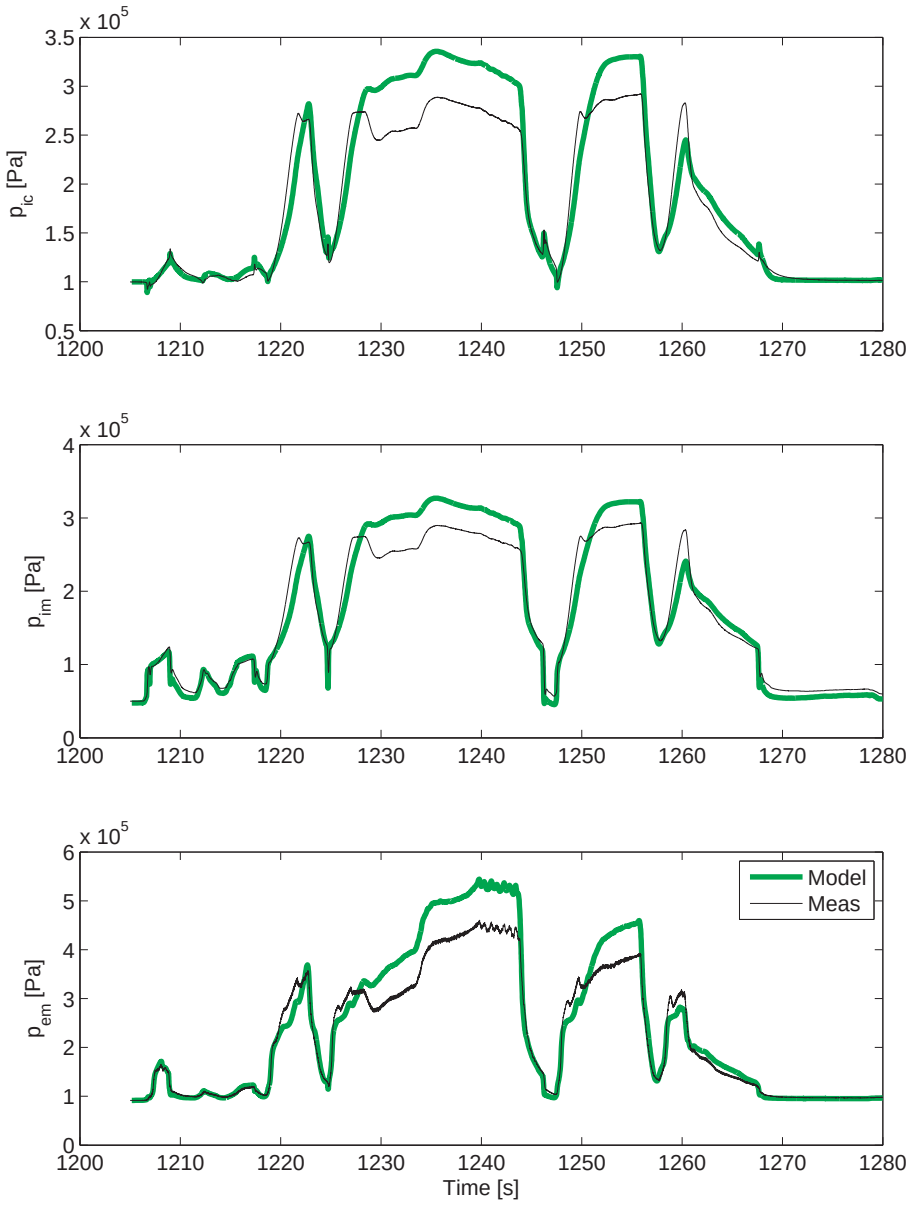

Figure 22: Comparison between diesel engine model simulation and dynamic validation data for some aggressive WHTC transients.

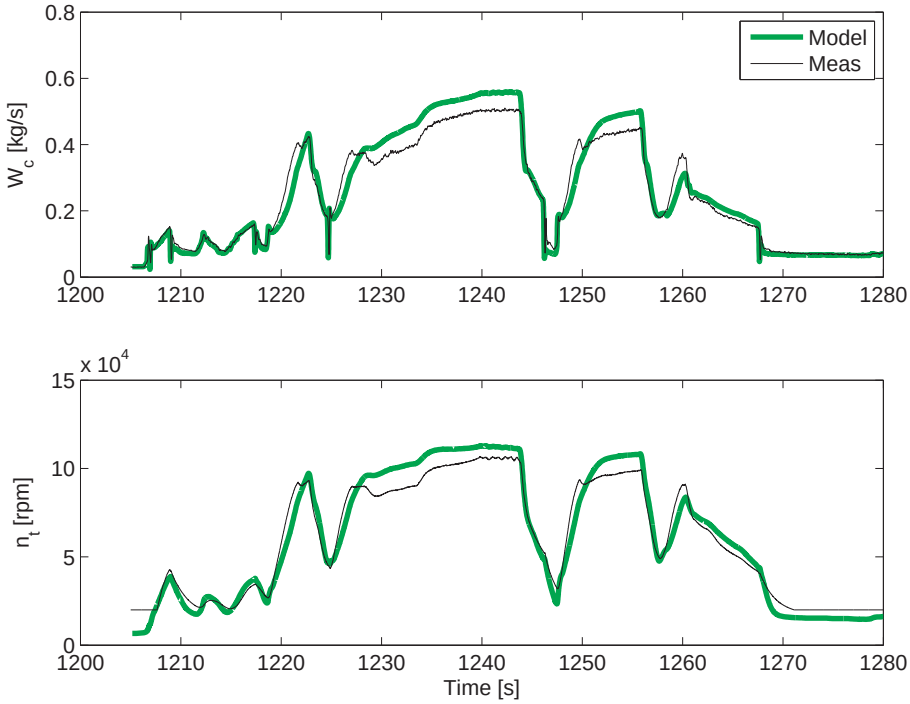

Figure 23: Comparison between diesel engine model simulation and dynamic validation data for some aggressive WHTC transients.

8 System analysis

An analysis of the characteristics and the behavior of a system aims at obtaining insight into the control problem. This is known to be important for a successful design of an EGR and VGT controller due to non-trivial intrinsic properties such as non-minimum phase behaviors and sign reversals, see for example [20]. Therefore, a system analysis of the proposed model is performed in the following sections. According to Sec. 1 it is natural to choose the oxygen/fuel ratio λ_O and the EGR-fraction x_{egr} as the main performance variables. Therefore, system properties for λ_O and x_{egr} are analyzed in Sec. 8.1 and 8.2.

8.1 Mapping of system properties for λ_O

A mapping of λ_O in steady state is shown in Fig. 24-26 covering the entire operating region at 20 different u_{vgt} points, 20 different u_{egr} points, 3 different u_{th} points, 3 different n_e points, and 3 different u_δ points. The black areas in the figures show the operating points where $\lambda_O < 1.2$ and these operating points shall be avoided by a controller, otherwise there will be to much smoke. This black area increases with decreasing u_{th} and for $u_{th} = 20\%$ in Fig. 26 $\lambda_O > 1.2$ only for $u_\delta = 60$ mg/cycle and for some few operating points with closed EGR and VGT positions.

Model responses to steps in VGT position and EGR-valve show that the DC-gains for the channels $u_{vgt} \to \lambda_O$ and $u_{egr} \to \lambda_O$ change sign with operating point. Knowledge about these sign reversals in the entire operating region is important when developing a control structure. Therefore, these sign reversals are also mapped in Fig. 24-26 by simulating step responses at each operating point. The sign reversals in $u_{vgt} \to \lambda_O$ and $u_{egr} \to \lambda_O$ are mapped by calculating the DC-gain in the step responses and then plotting the contour line where the DC-gain is equal to zero. The size of the steps in u_{vgt} and u_{egr} are 5% of the difference between two adjoining operating points. Note that the sign reversal for the channel $u_{vgt} \to \lambda_O$ occurs in operating points where the tangent to the contour line for λ_O is horizontal and that the sign reversal for the channel $u_{egr} \to \lambda_O$ occurs in operating points where the tangent to the contour line for λ_O is vertical. Fig. 24-26 show that the DC-gain for the channel $u_{vgt} \to \lambda_O$ has positive and negative sign in large operating regions. However, the DC-gain for the channel $u_{egr} \to \lambda_O$ has negative sign in a large operating region and positive sign in a small operating region.

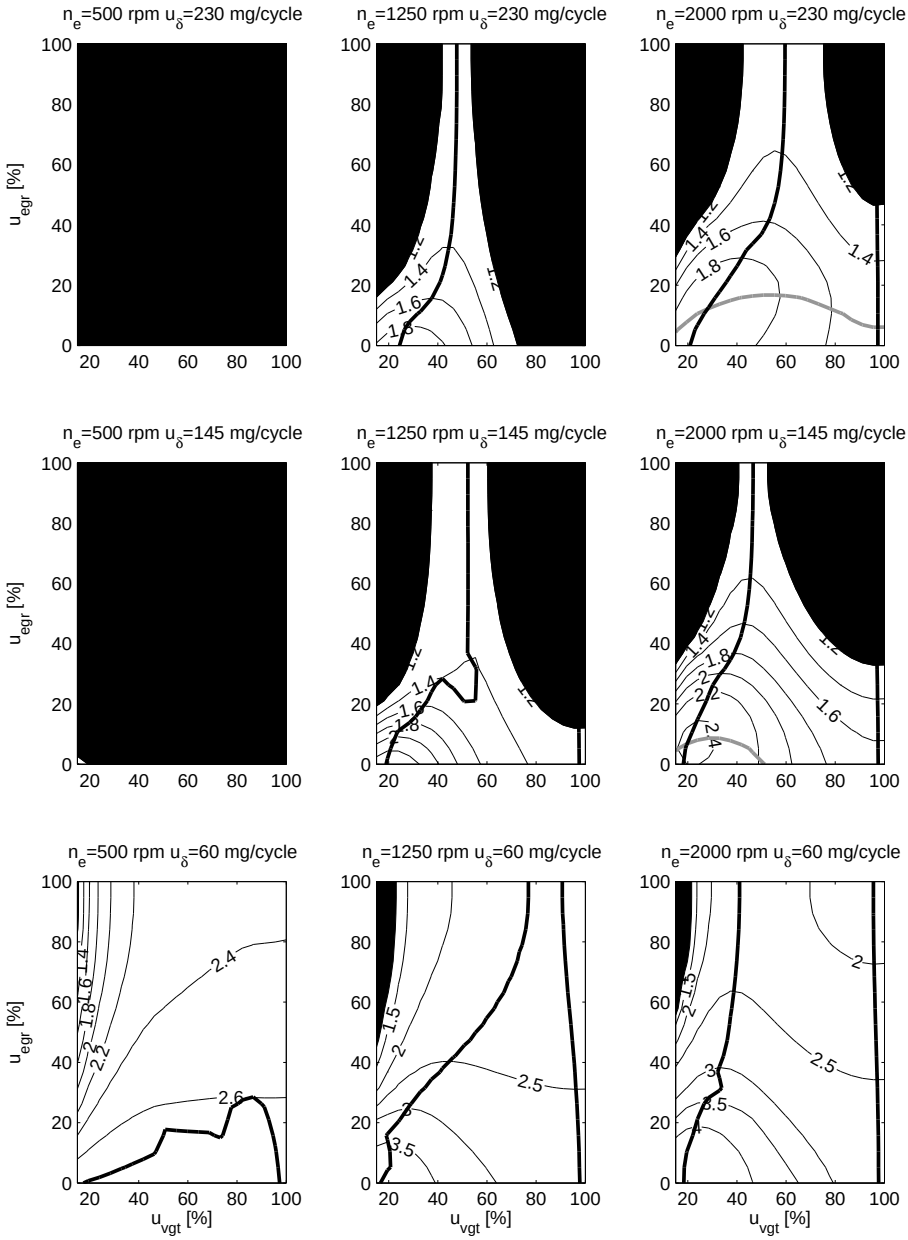

Figure 24: Contour plots of λ_O (thin black line) in steady state where $\lambda_O < 1.2$ in the black areas, and contour lines where the DC-gain is equal to zero for the channels $u_{vgt} \to \lambda_O$ (thick black line) and $u_{egr} \to \lambda_O$ (thick gray line) showing that sign reversals occur at these two thick lines. Intake throttle position: $u_{th} = 70\%$.

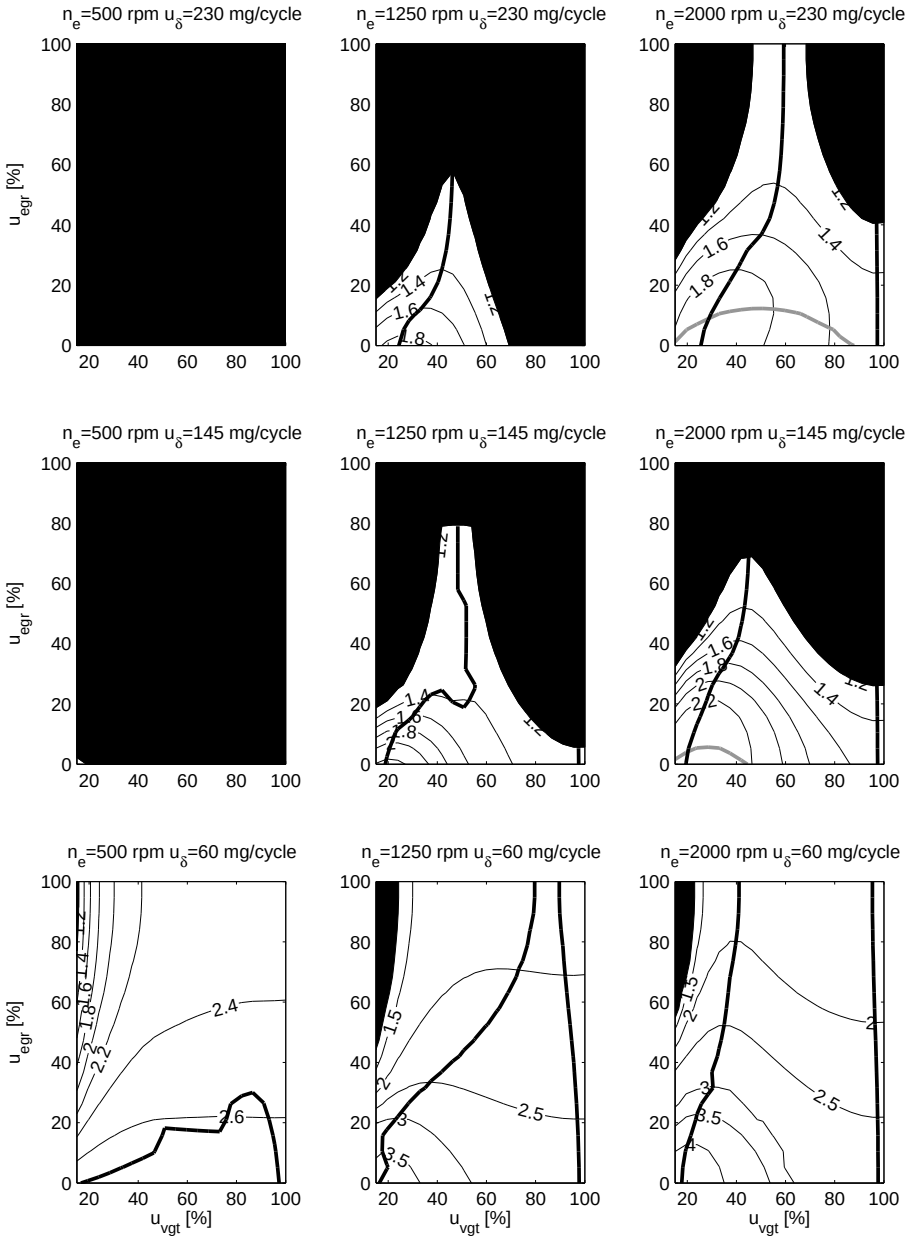

Figure 25: Contour plots of λ_O (thin black line) in steady state where $\lambda_O < 1.2$ in the black areas, and contour lines where the DC-gain is equal to zero for the channels $u_{vgt} \to \lambda_O$ (thick black line) and $u_{egr} \to \lambda_O$ (thick gray line) showing that sign reversals occur at these two thick lines. Intake throttle position: $u_{th} = 45\%$.

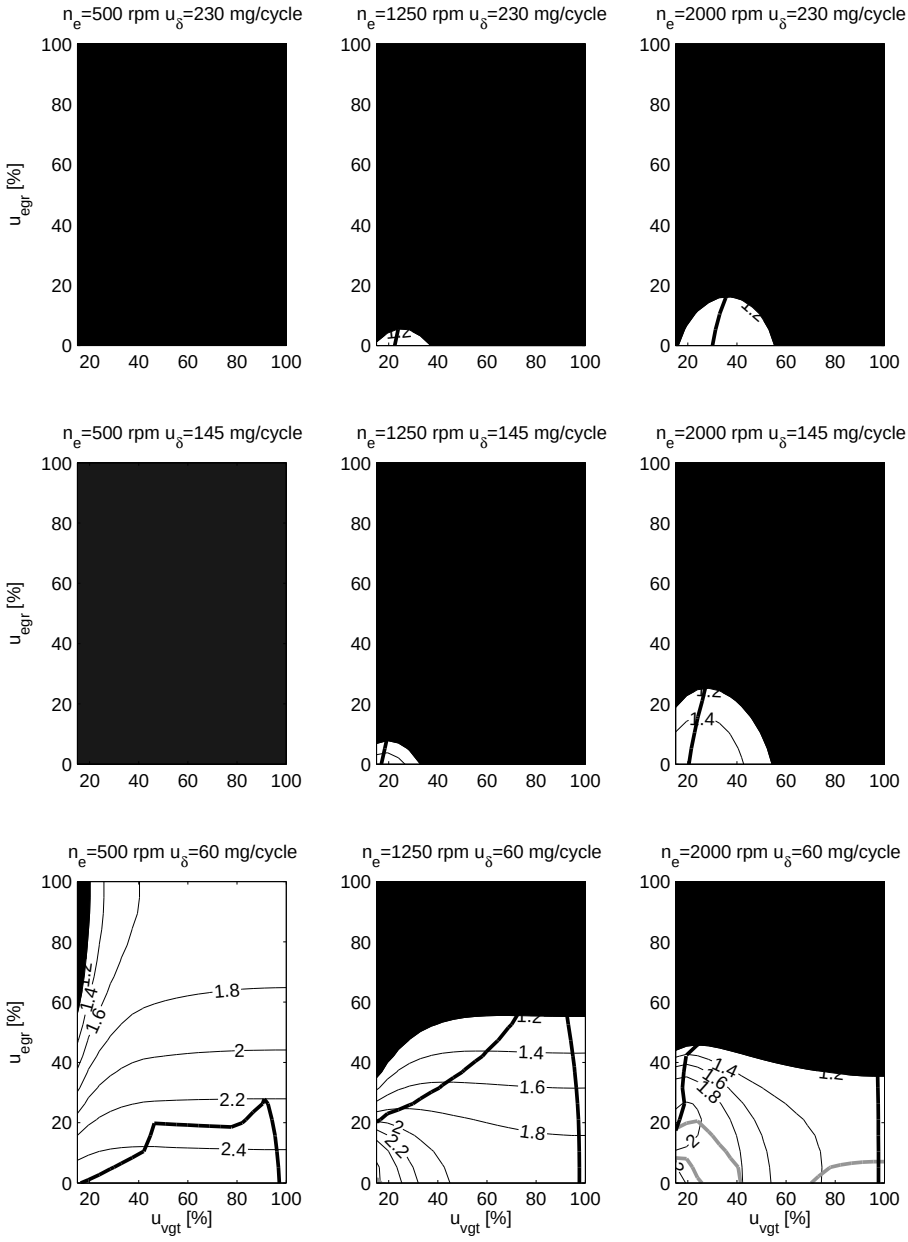

Figure 26: Contour plots of λ_O (thin black line) in steady state where $\lambda_O < 1.2$ in the black areas, and contour lines where the DC-gain is equal to zero for the channels $u_{vgt} \to \lambda_O$ (thick black line) and $u_{egr} \to \lambda_O$ (thick gray line) showing that sign reversals occur at these two thick lines. Intake throttle position: $u_{th} = 20\%$.

8.2 Mapping of system properties for x_{egr}

A mapping of x_{egr} in steady state is shown in Fig. 27-29 covering the entire operating region at 20 different u_{vgt} points, 20 different u_{egr} points, 3 different u_{th} points, 3 different n_e points, and 3 different u_δ points. The black areas in the figures show the operating points where $\lambda_O < 1.2$.

Model responses to steps in VGT position show that the DC-gain for the channel $u_{vgt} \rightarrow x_{egr}$ changes sign with operating point. This sign reversal is also mapped in Fig. 27-29 by simulating step responses at each operating point in the same way as in Fig. 24-26. Note that the sign reversal for the channel $u_{vgt} \rightarrow x_{egr}$ occurs in operating points where the tangent to the contour line for x_{egr} is horizontal. Fig. 27-29 show that the DC-gain for the channel $u_{vgt} \rightarrow x_{egr}$ has negative sign in a large operating region and positive sign in a small operating region.

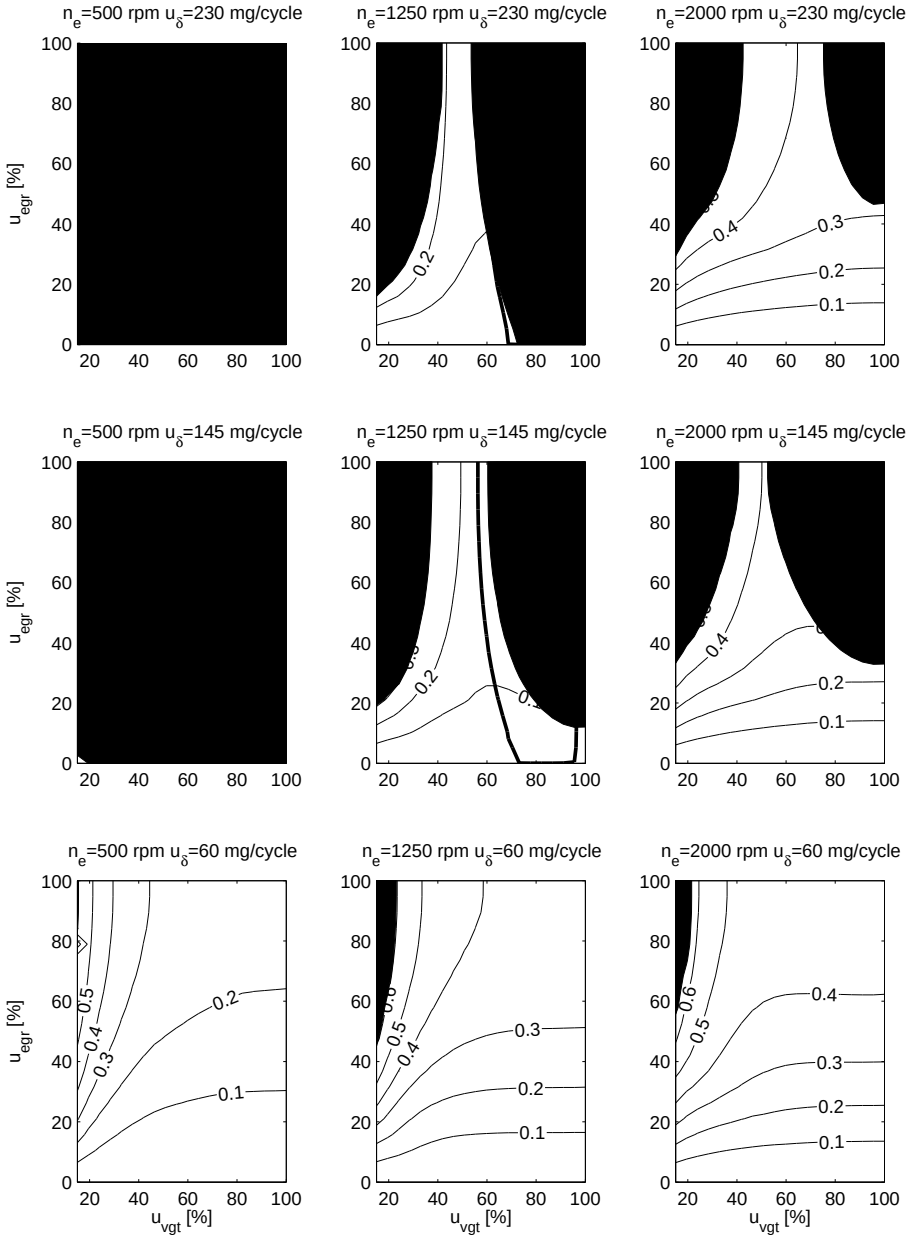

Figure 27: Contour plots of x_{egr} (thin black line) in steady state and contour lines where the DC-gain is equal to zero for the channel $u_{vgt} \rightarrow x_{egr}$ (thick black line) showing that a sign reversal occurs at this thick black line. $\lambda_O < 1.2$ in the black areas. Intake throttle position: $u_{th} = 70\%$.

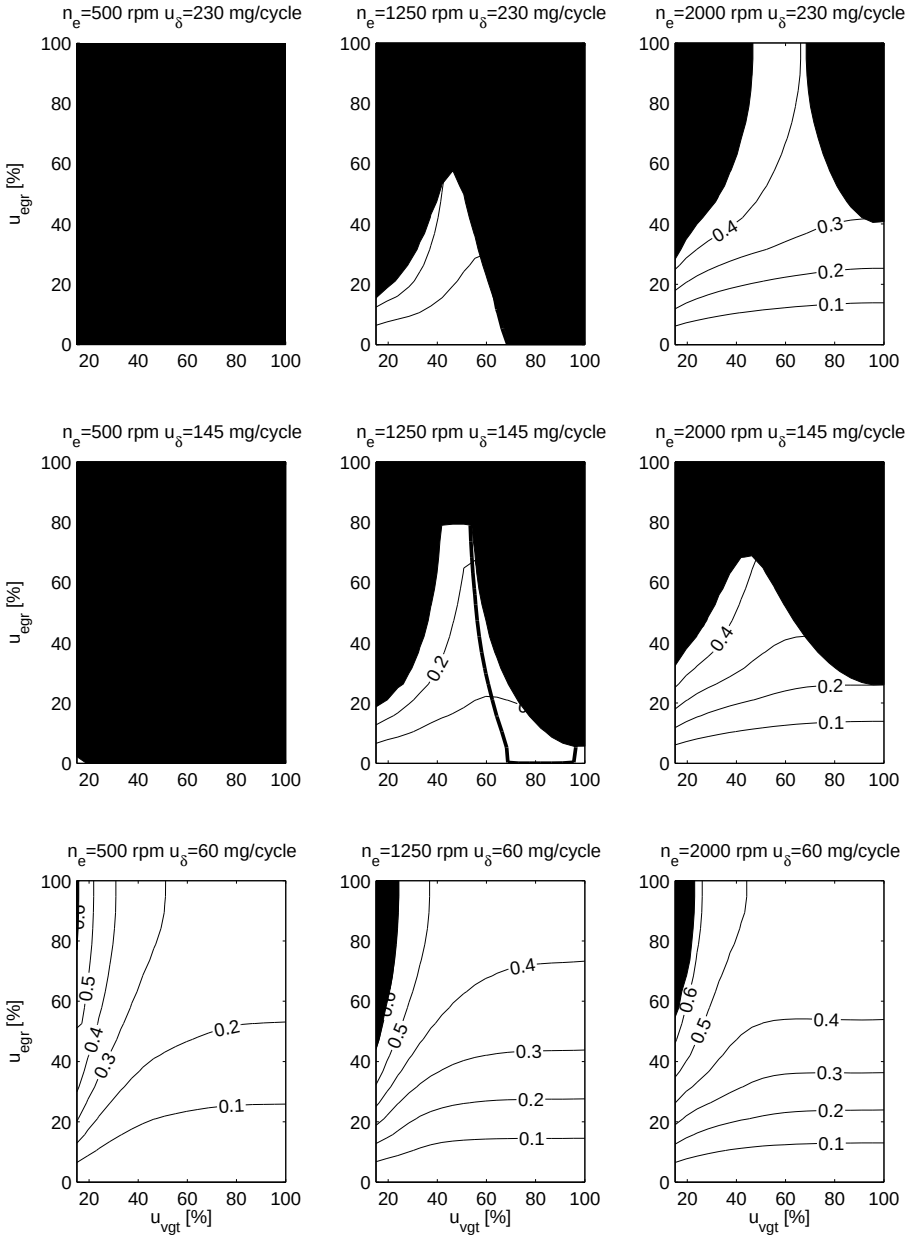

Figure 28: Contour plots of x_{egr} (thin black line) in steady state and contour lines where the DC-gain is equal to zero for the channel $u_{vgt} \to x_{egr}$ (thick black line) showing that a sign reversal occurs at this thick black line. $\lambda_O < 1.2$ in the black areas. Intake throttle position: $u_{th} = 45\%$.

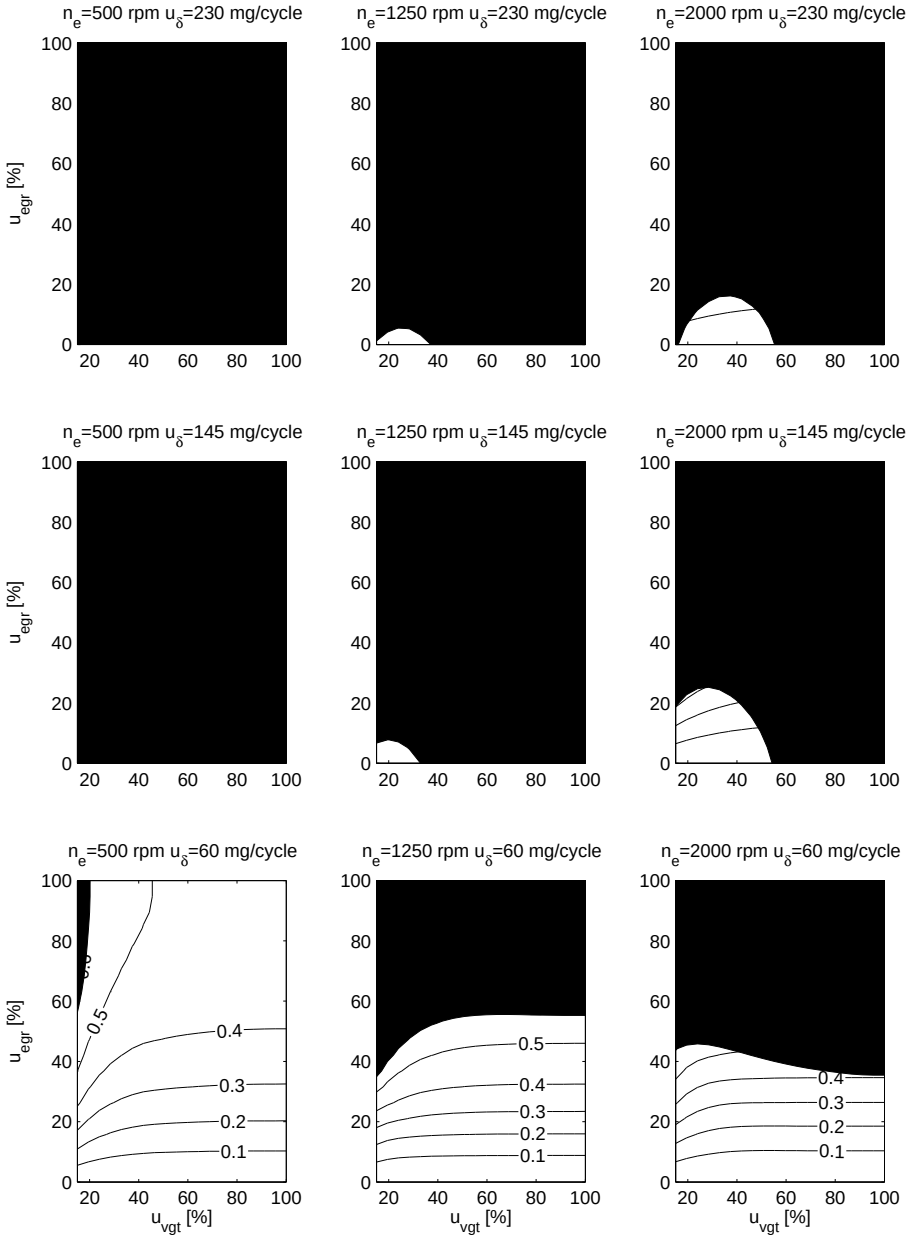

Figure 29: Contour plots of x_{egr} (thin black line) in steady state. $\lambda_O < 1.2$ in the black areas. Intake throttle position: $u_{th} = 20\%$.

9 Conclusions

A mean value model of a diesel engine with intake throttle, VGT, and EGR is developed and validated. The intended applications of the model are system analysis, simulation, and development of model-based control systems. The goal is to construct a model that describes the dynamics in the intercooler pressure, manifold pressures, turbocharger, EGR, and actuators with few states in order to have short simulation times. Therefore the model has only eleven states: intercooler, intake manifold, and exhaust manifold pressures, oxygen mass fraction in the intake and exhaust manifold, exhaust manifold temperature, turbocharger speed, and four states describing the actuator dynamics.

Model equations and parameters are described for each subsystem in the model. In order to have a low number of tuning parameters, flows and efficiencies are modeled using physical relationships and parametric models instead of look-up tables. All the model parameters are tuned automatically using several different least squares optimizations. In the optimization of the parameters in the static models it is important to tune both the sub-models and the complete model and not only the sub-models or not only the complete model.

Dynamic measurements and simulations show that the proposed model captures the essential system properties, i.e. non-minimum phase behaviors in the channels u_{egr} to p_{ic}, u_{egr} to p_{im}, u_{th} to p_{ic}, and u_{vgt} to n_t, and a non-minimum phase behavior, an overshoot, and a sign reversal in the channel u_{vgt} to W_c.

Static and dynamic validations of the entire model were performed using dynamic measurements of the complete World Harmonized Transient Cycle showing that the mean value of all absolute relative errors for all measured outputs are equal to 7.4 %.

A system analysis of the proposed model was performed in order to obtain insight into a VGT and EGR control problem where the goal is to control the performance variables oxygen fuel ratio λ_O and EGR-fraction x_{egr} using the VGT actuator u_{vgt} and the EGR actuator u_{egr}. Step responses over the entire operating region show that the channels $u_{vgt} \rightarrow \lambda_O$, $u_{egr} \rightarrow \lambda_O$, and $u_{vgt} \rightarrow x_{egr}$ have sign reversals.

References

[1] M. Ammann, N.P. Fekete, L. Guzzella, and A.H. Glattfelder. Model-based Control of the VGT and EGR in a Turbocharged Common-Rail Diesel Engine: Theory and Passenger Car Implementation. *SAE Technical paper 2003-01-0357*, January 2003.

[2] Per Andersson. *Air Charge Estimation in Turbocharged Spark Ignition Engines*. PhD thesis, Linköpings Universitet, December 2005.

[3] Å. Björk. *Numerical Methods for Least Squares Problems*. SIAM, 1996.

[4] M. Canova, P. Fiorani, and A. Gambarotta. A real-time model of a small turbocharged multijet diesel engine: application and validation. *SAE Technical paper 2005-24-065*, 2005.

[5] Alain Chevalier, Martin Müeller, and Elbert Hendricks. On the validity of mean value engine models during transient operation. *SAE Technical paper 2000-01-1261*, 2000.

[6] S.L. Dixon. *Fluid Mechanics and Thermodynamics of Turbomachinery*. Butterworth Heinemann, Woburn, 4:th edition, 1998.

[7] Economic Commission for Europe – Inland Transport Committee. Regulation no 49 of the economic commission for europe of the united nations (UN/ECE). Official Journal of the European Union, August 2010.

[8] Lars Eriksson. Mean value models for exhaust system temperatures. *SAE 2002 Transactions, Journal of Engines, 2002-01-0374*, 111(3), September 2002.

[9] Lars Eriksson. Modeling and control of turbocharged SI and DI engines. *Oil & Gas Science and Technology - Rev. IFP*, 62(4):523–538, 2007.

[10] Lars Eriksson, Lars Nielsen, Jan Brugård, Johan Bergström, Fredrik Pettersson, and Per Andersson. Modeling and simulation of a turbo charged SI engine. *Annual Reviews in Control*, 26(1):129–137, October 2002.

[11] Paolo Fiorani, Agostino Gambarotta, Gabriele Lucchetti, Francesco P. Ausiello, Matteo De Cesare, and Gabriele Serra. A detailed mean value model of the exhaust system of an automotive diesel engine. *SAE Technical paper 2008-28-0027*, 2008.

[12] Paolo Fiorani, Agostino Gambarotta, Marco Tonetti, and Enrico Lanfranco. A real-time model for the simulation of transient behaviour of automotive diesel engines. *SAE Technical paper 2006-01-3007*, 2006.

[13] L. Guzzella and A. Amstutz. Control of diesel engines. *IEEE Control Systems Magazine*, 18:53–71, 1998.

[14] Elbert Hendricks. Isothermal vs. adiabatic mean value SI engine models. In *IFAC Workshop: Advances in Automotive Control*, 2001.

[15] J.B. Heywood. *Internal Combustion Engine Fundamentals*. McGraw-Hill Book Co, 1988.

[16] M. Jankovic, M. Jankovic, and I.V. Kolmanovsky. Constructive lyapunov control design for turbocharged diesel engines. *IEEE Transactions on Control Systems Technology*, 2000.

[17] J.P. Jensen, A.F. Kristensen, S.C. Sorenson, N. Houbak, and E. Hendricks. Mean value modeling of a small turbocharged diesel engine. In *SAE Technical Paper 910070*, 1991.

[18] Andreas Jerhammar and Erik Höckerdal. Gas flow observer for a Scania diesel engine with VGT and EGR. Master's thesis, Linköpings Universitet, SE-581 83 Linköping, 2006.

[19] M. Jung. *Mean-Value Modelling and Robust Control of the Airpath of a Turbocharged Diesel Engine*. PhD thesis, University of Cambridge, 2003.

[20] I.V. Kolmanovsky, A.G. Stefanopoulou, P.E. Moraal, and M. van Nieuwstadt. Issues in modeling and control of intake flow in variable geometry turbocharged engines. In *Proceedings of* 18^{th} *IFIP Conference on System Modeling and Optimization*, Detroit, July 1997.

[21] M.J. Nieuwstadt, I.V. Kolmanovsky, P.E. Moraal, A.G. Stefanopoulou, and M. Jankovic. EGR–VGT control schemes: Experimental comparison for a high-speed diesel engine. *IEEE Control Systems Magazine*, 2000.

[22] R. Rajamani. Control of a variable-geometry turbocharged and wastegated diesel engine. *Proceedings of the I MECH E Part D Journal of Automobile Engineering*, November 2005.

[23] A.G. Stefanopoulou, I.V. Kolmanovsky, and J.S. Freudenberg. Control of variable geometry turbocharged diesel engines for reduced emissions. *IEEE Transactions on Control Systems Technology*, 8(4), July 2000.

[24] C. Vigild. *The Internal Combustion Engine Modelling, Estimation and Control Issues*. PhD thesis, Technical University of Denmark, Lyngby, 2001.

[25] Johan Wahlström. *Control of EGR and VGT for Emission Control and Pumping Work Minimization in Diesel Engines*. PhD thesis, Linköping University, 2009.

[26] Johan Wahlström and Lars Eriksson. Modeling of a diesel engine with VGT and EGR capturing sign reversal and non-minimum phase behaviors. Technical report, Linköping University, 2009.

[27] N. Watson and M.S. Janota. *Turbocharging the Internal Combustion Engine*. The Mechanical Press Ltd, Hong Kong, 1982.

A Notation

Table 6: Symbols used in the report

Symbol	Description	Unit
A	Area	m^2
BSR	Blade speed ratio	$-$
c_p	Spec. heat capacity, constant pressure	$J/(kg \cdot K)$
c_v	Spec. heat capacity, constant volume	$J/(kg \cdot K)$
J	Inertia	$kg \cdot m^2$
M	Torque	Nm
M_e	Engine torque	Nm
M_p	Pumping torque	Nm
n_{cyl}	Number of cylinders	$-$
n_e	Rotational engine speed	rpm
n_t	Rotational turbine speed	rpm
$(O/F)_s$	Stoichiometric oxygen-fuel ratio	$-$
p	Pressure	Pa
P	Power	W
q_{HV}	Heating value of fuel	J/kg
r_c	Compression ratio	$-$
R	Gas constant	$J/(kg \cdot K)$
R	Radius	m
T	Temperature	K
u_{egr}	EGR control signal. 100 - open, 0 - closed	%
u_{th}	Throttle control signal. 100 - open, 0 - closed	%
u_{vgt}	VGT control signal. 100 - open, 0 - closed	%
u_δ	Injected amount of fuel	$mg/cycle$
V	Volume	m^3
W	Mass flow	kg/s
x_{egr}	EGR fraction	$-$
X_O	Oxygen mass fraction	$-$
γ	Specific heat capacity ratio	$-$
η	Efficiency	$-$
λ_O	Oxygen-fuel ratio	$-$
Π	Pressure quotient	$-$
ρ	Density	kg/m^3
τ	Time constant	s
Φ_c	Volumetric flow coefficient	$-$
Ψ_c	Energy transfer coefficient	$-$
ω	Rotational speed	rad/s

Table 7: Indices used in the report

Index	Description
a	air
amb	ambient
bc	before compressor
c	compressor
d	displaced
e	exhaust
egr	EGR
ei	engine cylinder in
em	exhaust manifold
eo	engine cylinder out
ic	intercooler
f	fuel
$fric$	friction
ig	indicated gross
im	intake manifold
m	mechanical
t	turbine
tc	turbocharger
th	throttle
vgt	VGT
vol	volumetric
δ	fuel injection

Table 8: Abbreviations used in the report

Abbreviation	Description
EGR	Exhaust gas recirculation
VGT	Variable geometry turbocharger

B Simulink implementation